Keldysh Institute • Publication search

Keldysh Institute preprints • Preprint No. 12, 2010

T.Beuselinck, C.Van Bavinchove,
Sazonov V.V.

Some Tests of Acceleration Measurement Data Obtained Onboard FOTON M-3

Recommended form of bibliographic references: T.Beuselinck, C.Van Bavinchove, Sazonov V.V. Some Tests of Acceleration Measurement Data Obtained Onboard FOTON M-3. Keldysh Institute preprints, 2010, No. 12, 36 p. URL: **http://library.keldysh.ru/preprint.asp?id=2010-12&lg=e**

RUSSIAN ACADEMY OF SCIENCES
KELDYSH INSTITUTE OF APPLIED MATHEMATICS

T. Beuselinck, C. Van Bavinchove, V.V. Sazonov

SOME TESTS OF ACCELERATION MEASUREMENT DATA OBTAINED ONBOARD *FOTON M-3*

Moscow - 2010

Annotation

The paper presents the results of testing acceleration measurement data obtained by the accelerometer TAS3 onboard the spacecraft *Foton M-3* during its uncontrolled orbital flight in September, 2007. Testing was carried out in two ways. The first way consisted in comparison of the low-frequency component in the measurement data with the acceleration calculated along the reconstruction of spacecraft attitude motion, the reconstruction being found by processing onboard measurements of the Earth magnetic field. The second way used the low-frequency component in the acceleration measurement data as a source information for the alternative reconstruction of the spacecraft attitude motion. Then both reconstruction were compared with each other. Both ways took into account the correction of the acceleration data for the influence of magnetic field and some other corrections. The results, obtained in both ways, confirm the sufficiently high accuracy of the accelerometer TAS3 in the frequency range $0.0002 \div 0.002$ Hz.

Т. Бойзелинк, К. Ван Бавинхов, В.В. Сазонов. Проверка данных измерений микроускорения, полученных на борту КА "Фотон М-3". Приведены результаты тестирования данных измерений акселерометра TAS3, полученных во время неуправляемого орбитального полета спутника *Фотон М-3* в сентябре 2007 г. Тестирование выполнено двумя способами. В первом способе результаты низкочастотной фильтрации данных измерений сравниваются с результатами расчета микроускорения вдоль реконструкции вращательного движения спутника, найденной по данным бортовых измерений магнитного поля Земли. Во втором способе низкочастотная составляющая в данных измерений микроускорения используется для построения реконструкции вращательного движения спутника, и эта реконструкция сравнивается с реконструкцией, найденной по измерениям магнитного поля. В обоих способах в данные измерений акселерометра вносится поправка за влияние магнитного поля и ряд других поправок. Результаты, полученные обоими способами подтвердили достаточно высокую точность акселерометра TAS3 в диапазоне частот $0.0002 \div 0.002$ Гц.

1. Testing acceleration measurement data obtained in *Foton M-3*. The spacecraft *Foton M-3* had the measurement system DIMAC on its board. The system was designed and manufactured by the company RedShift Design and Engineering BVBA (Sint-Niklaas, Belgium). It supplied two kinds of measurement data suitable for reconstruction of the microgravity environment onboard the spacecraft. These were magnetic field and acceleration measurements. Magnetic field measurements proved to be rather accurate and enabled to reconstruct the spacecraft attitude motion [1]. The found reconstruction used for testing acceleration measurements in a low-frequency range. Such testing is based on the formula that expressed an acceleration at a given point of a spacecraft body through its kinematic parameters and some other quantities. Recall that formula.

Let a spacecraft be a rigid body, and let a point P be fixed with its frame. The difference between the gravitational field strength at the point P and the absolute acceleration of that point is called a (residual) acceleration at the point P. We denote the difference by $\mathbf{b}$. This quantity plays a part of $\mathbf{g}$ in orbital experiments. We assume that only the atmosphere drag is significant among nongravitational actions upon the spacecraft. Then $\mathbf{b}$ is defined by the formula [2]

$$\mathbf{b} = \mathbf{r} \times \dot{\boldsymbol{\omega}} + (\boldsymbol{\omega} \times \mathbf{r}) \times \boldsymbol{\omega} + \frac{\mu_e}{|\mathbf{R}|^3} \left[\frac{3\,(\mathbf{R} \cdot \mathbf{r})\,\mathbf{R}}{|\mathbf{R}|^2} - \mathbf{r} \right] + c\rho_a |\mathbf{v}| \mathbf{v}\,. \qquad (1)$$

Here, $\mathbf{r}$ is the radius vector of the point P with respect to the spacecraft center of mass, the point O; $\boldsymbol{\omega}$ is the absolute angular rate of the spacecraft; the dot above a symbol denotes differentiation with respect to time t; μ_e is the gravitational parameter of the Earth; $\mathbf{R}$ is the geocentric radius vector of the point O; $\mathbf{v}$ is the velocity of the point O with respect to the Earth surface; ρ_a is the atmosphere density at the point O; c is the spacecraft ballistic coefficient.

We used formula (1) in two ways. According to the first way, we reconstructed the spacecraft motion in a time interval with length of a few hours by magnetic measurements; we calculated the acceleration along the reconstruction by formula (1) in the point of accelerometer location. Then we compared the calculation results with the results of the low-frequency filtration of acceleration measurement data in the same interval. When both results were in a good agreement we supposed the acceleration filtered data were right [3]. The second way consisted in a direct use of the acceleration filtered data for a reconstruction of the spacecraft attitude motion [4]. We made such a reconstruction and compared it with the reconstruction based on processing the magnetic measurements. We realized both ways for the acceleration measurements obtained in *Foton M-2* [3, 4]. Below we describe similar results for the measurements made in *Foton M-3*.

2. Calculation of quasi-steady accelerations by reconstruction of spacecraft attitude motion. The method of the reconstruction consists in following [1]. We assign a time interval $t_0 \le t \le t_0 + T$ and, using the magnetic

measurements, construct in it the functions $\hat{h}_i(t)$ $(i = 1, 2, 3)$ approximating the components of the strength $\mathbf{H}$ of the local magnetic field in the spacecraft device coordinate system $y_1y_2y_3$. The axis y_1 is the longitudinal axis of the spacecraft; it is directed from the landing capsule to the device unit. We suppose that the local magnetic field coincides with the Earth one at the point O and calculate its components $H_i(t)$ $(i = 1, 2, 3)$ in the Greenwich coordinate system $Y_1Y_2Y_3$ along the spacecraft orbit basing on the analytical model IGRF. Certain relations should link two sets of functions obtained. The condition of the closest fit of these relations in the interval $t_0 \le t \le t_0 + T$ defines the solution of the spacecraft attitude motion equations that approximates the real motion.

The gravitational and some other torques are taken into account in those equations [1]. The equations are written in the coordinate system $x_1x_2x_3$ formed by the principal central axes of inertia of the spacecraft. The angles between the axes x_i and y_i did not exceed several degrees. Denote by $\| g_{ij} \|_{i,j=1}^{3}$ the matrix of transition from the system $x_1x_2x_3$ to the system $Y_1Y_2Y_3$, where g_{ij} was the cosine of the angle between the axes Y_i and x_j. The phase vector of the attitude motion equations consists of the quantities g_{1i}, g_{2i}, and the components ω_i of the spacecraft angular rate $\boldsymbol{\omega}$ in the system $x_1x_2x_3$ $(i = 1, 2, 3)$. The quantities g_{3i} are calculated by formulas $g_{31} = g_{12}g_{23} - g_{13}g_{22}$, etc. The matrix of transition from the system $x_1x_2x_3$ to the device coordinate system $y_1y_2y_3$ is denoted by $\| b_{ij} \|_{i,j=1}^{3}$. Here b_{ij} is the cosine of the angle between the axes y_i and x_j. We consider the solution of the motion equations minimizing the functional

$$\Phi = \sum_{i=1}^{3} \left\{ \sum_{n=0}^{N} \Big[\hat{h}_i(t_0 + ns) - h_i(t_0 + ns) \Big]^2 - (N+1)\Delta_i^2 \right\}, \qquad (2)$$

$$\Delta_i = \frac{1}{N+1} \sum_{n=0}^{N} [\, h_i(t_0 + ns) - h_i(t_0 + ns) \,], \quad s = \frac{T}{N},$$

$$h_i(t) = \sum_{j,k=1}^{3} H_j(t) g_{jk}(t) b_{ik}$$

as an reconstruction of the real attitude motion of the spacecraft in the interval $t_0 \le t \le t_0 + T$. Functional (2) is minimized on the initial conditions of the solution at the point t_0 and parameters of the mathematical model. The latter include some parameters of the motion equations and three angles specifying the transition matrix $\| b_{ij} \|$. Usually, we take $T = 100 \div 400$ min and $s \approx 1$ min. Examples of the reconstructions, obtained in this way, are presented in [1].

Figs. 1a, 1b, and 1c contain the plots (lines without marks) of acceleration components b_i $(i = 1, 2, 3)$ calculated by formula (1) for three time interval from [1]. The components relate to the system $y_1y_2y_3$. Calculations were made for

the point $P = (0.074\,\mathrm{m}, -0.184\,\mathrm{m}, -0.307\,\mathrm{m})$ in that system. The accelerometer TAS3, a unit of the system DIMAC, was located near this point.

3. Filtration of low-frequency component from TAS3 data. The accelerometer TAS3 operated continuously during the whole flight. It measured an apparent acceleration $(-\mathbf{b})$ and was located near the furnace POLIZON. Its sensitive axes were parallel to the axes of the device coordinate system but axes 1 and 3 (x and z) had opposite directions. TAS3 produced the data in a wide spectral range. They have a sample rate equal to 1000 readings per second. We investigate below only the low-frequency component of these data. Our purpose is to compare it with the acceleration calculated by formula (1).

Comparison is justified if both functions have approximately the same spectrum. It means we have to extract from the measured data the component with frequencies of no more than some hundredths of a hertz. The extraction, i.e., the low-frequency filtration, was made by using discrete Fourier series independently for each vector component.

Let M and N be natural numbers, and x_k $(k = 0, 1, \ldots, MN)$ be a segment of the measurement data of any acceleration component. The measurement x_k was made at the instant $t_0 + k\Delta t$, $\Delta t > 0$. The low-frequency component, contained in these data, was represented by the following expression

$$x(t) = a_N + a_{N+1}\,(t - t_0) + \sum_{n=1}^{N-1} a_n \sin \frac{\pi n (t - t_0)}{NM\Delta t}\,, \tag{3}$$

where a_n are coefficients. These coefficients were found by the least squares method. To calculate them, the simple explicit formulas are available [2]. Some oscillations with relatively high frequencies are often revealed in expression (3), which was obtained in this way. In order to remove them, the coefficients a_n at highest harmonics in (3) were multiplied by the factors $(N-n)/(N-N_1)$, where N_1 is the integer part of the number $N/2$ and $n = N_1 + 1, \ldots, N - 1$. We didn't use expressions (3) directly but dealt with their values

$$\tilde{x}_n = x(t_n)\,, \quad t_n = t_0 + n\delta t \quad (n = 0, 1, \ldots, N)\,, \quad \delta t = M\Delta t. \tag{4}$$

We call these values the filtered data and denote their vector components by $B_i(t)$ $(i = 1, 2, 3)$. The functions $B_i(t)$ are defined on the mesh $\{t_n\}$.

In the examples below, expressions (3) were constructed using data segments with a length of 360 min. The segments correspond to intervals 10, 14, and 16 considered in [1]. The above procedure was applied at $\Delta t = 0.001$ s, $M = 30000$, and $N = 720$. The spectrum of functions, obtained in this way, lies within the limits from 0 to 0.017 Hz. TAS3 measurements have erroneous constant biases in each their vector component and so we changed values of the coefficients a_N to have zero means of data (4).

Figs. 1a, 2a, and 3a allow to compare the low-frequency component in TAS3 measurements with its calculated analog. The plots, marked by daggers, present the results of the filtration; the plots without daggers represent the results of calculation by formula (1). The marked functions were obtained from the respective data (4) by the following modifications. First we changed the sign of the function $B_2(t)$ (thereby we made the transform $-\mathbf{b} \to \mathbf{b}$). Then we added the constant biases Δ_{bi} to the functions $B_i(t)$ to obtain the equalities $\langle B_i + \Delta_{bi} \rangle = \langle b_i \rangle$ $(i = 1, 2, 3)$. Here we use the notation

$$\langle f \rangle = \frac{1}{N+1} \sum_{n=0}^{N} f(t_n)$$

for any function $f(t)$ defined on the mesh $\{t_n\}$.

One can see from the figures that vector components b_1 of calculated and filtered accelerations are closed when amplitudes of their oscillations are sufficiently large. Coincidence of components b_1 in Figs. 2a, 3a is good. Their coincidence in Fig. 1a is worse. It is difficult to say about any coincidence in the case of vector components b_2 and b_3 for calculated and filtered accelerations.

4. Correction of filtered TAS3 measurement data. The discrepancy of filtered acceleration data and their calculation analog was explained in [3]. It is due to the influence of the Earth magnetic field on the accelerometer. We can compensate this influence by the transformation

$$B_i - \sum_{j=1}^{3} m_{ij} h_j \to B_i \quad (i = 1, 2, 3)\,,$$

where m_{ij} are constants. We suppose here and below that the sign of the component B_2 has been changed. If we make the correction for the magnetic field, it is naturally to make simultaneously some other corrections [3]. Namely the correction for infra low-frequency errors, the correction for the shift of TAS3 time scale, the correction of the spacecraft ballistic coefficient, and the correction for misalignment of the TAS3 sensitive axes with respect to the axes y_i. We specify the later correction by the vector $\boldsymbol{\vartheta} = (\vartheta_1, \vartheta_2, \vartheta_3)$ of infinitesimal rotation of the TAS3 axes with respect to the system $y_1 y_2 y_3$. The components of $\boldsymbol{\vartheta}$ regards both to the system $y_1 y_2 y_3$ and to the system formed by the corresponding sensitive axes of TAS3. The correction of the ballistic coefficient c is specified by means of multiplication of c by the factor χ: $\chi c \to c$. This correction compensates short time variations of c and ρ_a within a long interval, in which c was defined. Taking into account all these correction and assuming they allow to remove all possible errors, we can write

$$B_1(t) + \vartheta_2 B_3(t) - \vartheta_3 B_2(t) - Z_1(t) - \sum_{j=1}^{3} m_{1j} h_j(t + \tau_b) =$$

$$= \sum_{j=1}^{3} c_{1j}(t+\tau_b)[x_j^{(1)} + x_j] + \chi b_1^{(a)}(t+\tau_b)\,,$$

$$B_2(t) + \vartheta_3 B_1(t) - \vartheta_1 B_3(t) - Z_2(t) - \sum_{j=1}^{3} m_{2j} h_j(t+\tau_b) =$$

$$= \sum_{j=1}^{3} c_{2j}(t+\tau_b)[x_j^{(2)} + x_j] + \chi b_2^{(a)}(t+\tau_b)\,, \qquad (5)$$

$$B_3(t) + \vartheta_1 B_2(t) - \vartheta_2 B_1(t) - Z_3(t) - \sum_{j=1}^{3} m_{3j} h_j(t+\tau_b) =$$

$$= \sum_{j=1}^{3} c_{3j}(t+\tau_b)[x_j^{(3)} + x_j] + \chi b_3^{(a)}(t+\tau_b)\,,$$

$$Z_i(t) = A_i^{(K+1)} + (t-t_0)A_i^{(K+2)} + \sum_{k=1}^{K} A_i^{(k)} \sin\frac{\pi k(t-t_0)}{N\delta t}\,.$$

Here, the functions $Z_i(t)$ compensate infra low-frequency errors in TAS3 data; τ_b is the shift of DIMAC time scale with respect to the time scale used for description of the spacecraft attitude motion; the functions $c_{ij}(t)$ and $b_j^{(a)}(t)$ are defined by relations (see (1), $\mathbf{e}_i$ are unit vectors along the axes y_i)

$$\mathbf{e}_i \times \dot{\boldsymbol{\omega}} + (\boldsymbol{\omega} \times \mathbf{e}_i) \times \boldsymbol{\omega} + \frac{\mu_e}{|\mathbf{R}|^3}\left[\frac{3\,(\mathbf{R}\cdot\mathbf{e}_i)\,\mathbf{R}}{|\mathbf{R}|^2} - \mathbf{e}_i\right] = \sum_{j=1}^{3} c_{ji}\mathbf{e}_j\,,$$

$$c\rho_a|\mathbf{v}|\mathbf{v} = \sum_{j=1}^{3} b_j^{(a)}\mathbf{e}_j\,;$$

the quantities x_j set the origin of TAS3 coordinate system with respect to the spacecraft mass center; $x_j^{(k)}$ $(j = 1, 2, 3)$ are the coordinates of the TAS3 sensor for the axis y_k in the TAS3 own coordinate system:

$$\begin{aligned}
&x_1^{(1)} = -56.2\,\text{mm}, \quad x_2^{(1)} = 48.5\,\text{mm}, \quad x_3^{(1)} = -57.0\,\text{mm},\\
&x_1^{(2)} = -36.5\,\text{mm}, \quad x_2^{(2)} = 22.3\,\text{mm}, \quad x_3^{(2)} = -70.5\,\text{mm},\\
&x_1^{(3)} = -31.0\,\text{mm}, \quad x_2^{(3)} = 48.5\,\text{mm}, \quad x_3^{(3)} = -27.8\,\text{mm}.
\end{aligned}$$

We considered relations (5) as a means for determining the unknown constants ϑ_i, x_i, $A_i^{(k)}$, m_{ij}, χ, and τ_b. We look for these quantities in the following way. Let τ_b be given. We consider relations (5) at the points t_n defined by formulas

(4). The quantities $B_i(t_n)$ have been calculated by the filtration; the quantities $c_{ij}(t_n+\tau_b)$ and $b_i^{(a)}(t_n+\tau_b)$ are calculated by interpolation with the aid of finite Fourier series. Those series have been constructed basing on a proper solution of the spacecraft motion equations. We obtain as a result the overdetermined linear system with the unknown quantities ϑ_i, x_i, $A_i^{(k)}$, m_{ij}, and χ. We treat the problem of finding its solution as a standard linear regression problem. We solve it by the least squares method for each τ_b in the uniform mesh with the step 1 s and calculate the standard deviation $\sigma_b(\tau_b)$ of discrepancies in (5). The value $\tau_b^* = \operatorname{argmin}\, \sigma_b(\tau_b)$ is considered to be the required estimate of τ_b; the solution of the regression problem at $\tau_b = \tau_b^*$ gives the required estimates of the quantities listed above. The standard deviations of these quantities, calculated at fixed $\tau_b = \tau_b^*$, are adopted as accuracy characteristics of the found estimates. We emphasize the standard deviations are calculated at fixed τ_b and are so-called conditional standard deviations. The unconditional standard deviation σ_τ of the estimate τ_b^* is calculated by the formula

$$\sigma_\tau^2 = 2\sigma_b^2(\tau_b^*)\left[(3N-3K-20)\,\frac{d^2\sigma^2(\tau_b^*)}{d\tau_b^2}\right]^{-1}.$$

Figs. 1, 2, and 3 with indices 'b' and 'c' illustrate some solutions of the regression problem at $K=5$. Figs. 1b, 2b, and 3b contain the plots of the functions $\hat{b}_i(t)$ and $b_i(t)$ $(i=1,2,3)$, which are defined by the left-hand and right-hand sides of formulas (5) respectively. The plots of the functions $\hat{b}_i(t)$ are marked by daggers. These functions represent the corrected measurement data. The functions $b_i(t)$ are the calculated analog of the functions $\hat{b}_i(t)$. Figs. 1c, 2c, and 3c contain the plots of the differences $\Delta b_i(t) = \hat{b}_i(t) - b_i(t)$ $(i=1,2,3)$. The functions $\hat{b}_i(t)$ and $b_i(t)$ are in a good agreement with each other. The differences $\Delta b_i(t)$ are small and look as irregular oscillations with sufficiently high frequencies. The figure captions contain the values of σ_b, τ_b, and σ_τ. These quantities for various interval are in a good agreement too.

We don't quote all results obtained by solving the regression problem because according to [1] this approach gives acceptable results only for large $|\boldsymbol{\omega}|$. Therefore we list only the results related to the interval shown in Fig. 3:

$$\chi = 0.922\,(0.016),$$

$$\vartheta_1 = -0.043\,(0.011), \quad \vartheta_2 = -0.050\,(0.0033), \quad \vartheta_3 = 0.005\,(0.0027),$$

$$x_1 = 21.7\,(0.57)\,\text{cm}, \quad x_2 = -23.1\,(0.092)\,\text{cm}, \quad x_3 = -24.6\,(0.092)\,\text{cm},$$

$$\| m_{ij} \| = \left\| \begin{array}{ccc} -186.4\,(1.3) & -112\,(1.4) & -180\,(1.4) \\ 4\,(1.3) & -164\,(1.5) & -113\,(2.3) \\ -29\,(1.3) & -54\,(2.3) & -148\,(1.9) \end{array} \right\|.$$

Here, the unit of ϑ_i is radian, the unit of m_{ij} is $10^{-7}\mathrm{m}/(\mathrm{s}^2 \cdot \mathrm{Oe})$, the numbers in brackets are respective standard deviations.

5. Pared-down mathematical model of spacecraft attitude motion [4]. The spacecraft is assumed to be an axially symmetric rigid body. To write equations of its motion and relations, used in processing measurement data, we introduce four right-hand Cartesian coordinate systems. Two of these systems are the same that were defined in Section 2. They are the Greenwich system $Y_1Y_2Y_3$ and the spacecraft fixed system $x_1x_2x_3$. We assume additionally to Section 2 that the axis x_1 is a spacecraft axis of symmetry so the spacecraft inertia tensor has the matrix $\mathrm{diag}\,(I_1, I_2, I_2)$ in the system $x_1x_2x_3$.

Two another coordinate systems are the auxiliary system $z_1z_2z_3$ and the quasi inertial system $X_1X_2X_3$. The auxiliary system serves for writing down the equations of spacecraft attitude motion. The axis z_1 coincides with the axis x_1. The axes x_2 and x_3 are obtained from the axes z_2 and z_3 by rotating the system $z_1z_2z_3$ through the angle φ around the axis z_1. To specify a kinematic relation between the systems $x_1x_2x_3$ and $z_1z_2z_3$ we assume that the absolute angular rate of the latter system has zero component along the axis z_1. Let w_2, w_3 be components of this angular rate along the axes z_2, z_3 and let the spacecraft absolute angular rate $\boldsymbol{\omega}$ has components $(\omega_1, \omega_2, \omega_3)$ in system $x_1x_2x_3$. Then $\dot{\varphi} = \omega_1$ and

$$\omega_2 = w_2 \cos\varphi + w_3 \sin\varphi\,, \quad \omega_3 = -w_2 \sin\varphi + w_3 \cos\varphi\,. \tag{6}$$

The quasi inertial system $X_1X_2X_3$ serves for graphic representation of the spacecraft attitude motion. The axis X_2 is directed along the vector $\mathbf{R} \times \dot{\mathbf{R}}$ at every instant; the axis X_3 lies in the plane Y_1Y_2 and is directed to the ascending node of the spacecraft osculating orbit. The absolute value of the angular rate of this system did not exceed 5° per day.

We denote the transition matrix from the system $z_1z_2z_3$ to the Greenwich system by $\| g_{ij} \|_{i,j=1}^3$. Here g_{ij} is the cosine of the angle between the axes Y_i and z_j. The matrix elements are expressed as functions of the angles γ_g, δ_g, and β_g, which are defined in the following way. The system $Y_1Y_2Y_3$ can be transformed to the system $z_1z_2z_3$ by three sequential rotations (we suppose all coordinate origins are in the same point O, the spacecraft mass center): 1) through the angle $\delta_g + \pi/2$ around the axis Y_2, 2) through the angle β_g around the new axis Y_3, 3) through the angle γ_g around the new axis Y_1, which coincides with the axis z_1.

We specify the attitude of the system $z_1z_2z_3$ with respect to the system $X_1X_2X_3$ by the angles γ, δ, and β, which are defined similarly to the angles γ_g, δ_g, β_g.

The complete system of the spacecraft motion equations consists of two subsystems. The first subsystem describes the motion of the point O and coincides with the analogous subsystems in [1, 4]. The second subsystem describes the

rotation of the system $z_1z_2z_3$. This subsystem consists of Poisson's kinematic equations for the first two rows of the matrix $\parallel g_{ij} \parallel$ as well as Euler's dynamic equations for the angular rates w_2, w_3. We take into account four external torques in Euler's equations: 1) gravitational torque, 2) restoring aerodynamic torque, 3) torque from the Earth magnetic field, 4) constant torque permanently directed along the axis x_1. Calculating the aerodynamic torque, we assume the external envelope of the spacecraft is a sphere, its center being in the axis x_1. Calculating the torque from the Earth magnetic field, we assume the own spacecraft dipole moment is parallel to the axis x_1. The second subsystem has the form

$$
\begin{gathered}
\dot w_2 + \lambda\,\omega_1 w_3 = -\frac{3\mu_e}{R^5}(1-\lambda)z_1z_3 + pE\rho_a v v_3 - mh_3'\,,\\
\dot w_3 - \lambda\,\omega_1 w_2 = \quad \frac{3\mu_e}{R^5}(1-\lambda)z_1z_2 - pE\rho_a v v_2 + mh_2'\,,\\
\dot g_{11} + w_2 g_{13} - w_3 g_{12} = \omega_e g_{21}\,, \qquad (7)\\
\dot g_{12} + w_3 g_{11} = \omega_e g_{22}\,, \quad \dot g_{13} - w_2 g_{11} = \omega_e g_{23}\,,\\
\dot g_{21} + w_2 g_{23} - w_3 g_{22} = -\omega_e g_{11}\,,\\
\dot g_{22} + w_3 g_{21} = -\omega_e g_{12}\,, \quad \dot g_{23} - w_2 g_{21} = -\omega_e g_{13}\,,\\
\omega_1 = \Omega + \varepsilon(t-t_0)\,,\ \lambda = \frac{I_1}{I_2}\,,\ R = \sqrt{z_1^2+z_2^2+z_3^2}\,,\ v = \sqrt{v_1^2+v_2^2+v_3^2}\,.
\end{gathered}
$$

Here, z_i, v_i, and h_i' are the components of the vectors $\mathbf{R}$, $\mathbf{v}$, and $\mathbf{H}$ (see Sections 1 and 2) in the system $z_1z_2z_3$; the parameters p and m specify the aerodynamic and magnetic torques respectively; εI_1 is the constant torque along the axis x_1; ω_e is the angular rate of the Earth rotation; E is the scale factor. We use in (7) the explicit solution of the equation $\dot\omega_1 = \varepsilon$, Euler's equations for ω_1; Ω is a parameter; a choice of the instant t_0 will be specified below.

We use 1000 s as a unit of time and 1000 km as a unit of length at numerical integrating equations (7). Then the units of the other quantities are following: $[v_i] =$ km/s, $[\omega_i] = [w_i] = 10^{-3}\mathrm{s}^{-1}$, $[p] = \mathrm{cm/kg}$, $[h_i'] = 0.1\mathrm{Oe}$, $[m] = 10^{-5}\mathrm{Oe}^{-1}\mathrm{s}^{-2}$, $[\varepsilon] = 10^{-6}\mathrm{s}^{-2}$, $[\rho_a] = \mathrm{kg/m}^3$, $E = 10^{10}$. The atmosphere density is calculated according to model [5]. The Earth magnetic field is calculated according to the analytical model IGRF. The third row of the transition matrix $\parallel g_{ij} \parallel$ is calculated at integration as a cross-product of its two first rows. We define a motion of the system $x_1x_2x_3$ and the functions $\omega_2(t)$, $\omega_3(t)$ for a solution of equations (7) by the relation $\varphi = \Omega(t-t_0) + \varepsilon(t-t_0)^2/2$ and formulas (6). The variables g_{1i} and g_{2i} are not independent owing to orthogonality of the matrix $\parallel g_{ij} \parallel$. The initial values of g_{1i} and g_{2i} are expressed in terms of the angles γ_g, δ_g, and β_g on this reason.

The parameter λ in (7) is known: $\lambda = 0.255$. The parameters p, m, and ε are estimated by processing measurement data along with initial values of a

spacecraft attitude motion, i. e., they are fitted parameters. We have also the variant of data processing, in which λ is among the fitted parameters.

Equations (7) and some other mathematical models, used below, are simpler than analogous models in [1] and in Sections 2, 4. We did that to reduce the total number of fitted parameters and to avoid the use of a priori information and regularization techniques in statistical procedures. To compensate this simplification we content ourselves with processing of simple spacecraft motions when the angular rate ω_1 is sufficiently large.

6. Statistical technique of reconstruction of *Foton M-3* attitude motion by magnetic field measurements. Equations (7) were successfully used for processing measurement data obtained in *Foton M-2* and *Foton-12* [4, 6]. But their using restricted oneself to motions with large values of ω_1. *Foton M-3* had lesser values of this quantity. So we had to test equations (7) by data from *Foton M-3* specially. We used for testing the magnetic field measurements. This testing proved to be successful and provided us with a bench-mark to check the acceleration measurement. We processed the magnetic measurements by the technique [4], which was similar to the technique mentioned in Section 2. We use below notations of that section without any explanation.

We assume that the system $y_1y_2y_2$, which is used for interpretation of the magnetic measurements, coincides with the system $x_1x_2x_3$. The transition matrix from the system $x_1x_2x_3$ to the system $z_1z_2z_3$ has the form

$$\| b_{ij} \|_{i,j=1}^{3} = \left\| \begin{array}{ccc} 1 & 0 & 0 \\ 0 & \cos\varphi & \sin\varphi \\ 0 & -\sin\varphi & \cos\varphi \end{array} \right\| .$$

Here, b_{ij} is the cosine of the angle between the axes z_i and x_j.

Following the least squares method, we consider a solution of system (7) as a reconstruction of the real spacecraft motion in the interval $t_0 \le t \le t_0 + T$ if it provides minimum to functional (2), where the matrices $\| g_{ij} \|$ and $\| b_{ij} \|$ have the just defined form. At that, we use the initial point t_0 of the processed interval as the instant t_0 in (7). Functional (2) is minimized over 9 quantities: p, m, ε, Ω, $w_2(t_0)$, $w_3(t_0)$, $\gamma_g(t_0)$, $\delta_g(t_0)$, $\beta_g(t_0)$. The first four quantities specify system (7), the other quantities specify its solution.

We solve the minimization problem by Gauss–Newton's method and use appropriate standard deviations to characterize the accuracy of approximating the processed data and scattering the fitted quantities. The standard deviations are calculated in the following manner. Let $\Phi_{\min}$ be the value of functional (2) at its minimum point, C be the matrix of Gauss–Newton's normal equations at that point ($2C$ is approximately equal to the matrix of the quadratic form $d^2\Phi$ at the minimum point of Φ). Then the standard deviation of errors in processed data is estimated by the quantity

$$\sigma_H = \sqrt{\frac{\Phi_{\min}}{3N-9}}\,.$$

The standard deviations of the fitted parameters are equal to the square roots of corresponding diagonal elements of the matrix $\sigma_H^2 C^{-1}$. We denote the standard deviations of the parameters p, m, and ε by σ_p, σ_m, and σ_ε.

7. Real attitude motion of *Foton M-3*. The technique above was applied for reconstructing the spacecraft motion in 5 time intervals. Some results are presented in Table 1 and in Figs. 4a, 5a, ..., 8a. The table contains certain characteristics of the intervals and the solutions of system (7) that approximate the motion. In particular, it contains the parameters p, m, ε, and the standard deviations σ_H, σ_p, σ_m, σ_ε. The first column of the table contains (in brackets) the days of September 2007 that contains the respective interval. Interval 1 was processed at $\lambda = 0.286$; the others intervals were processed at $\lambda = 0.255$. The special value of λ for interval 1 was found by minimization of functional (2) over 10 quantities: λ and 9 parameters listed in Section 6. These change of λ compensates the operation of the BIOBOX centrifuge: the centrifuge operated in interval 1 and was turning off in the other intervals.

Figs. 4a, ..., 8a illustrate the accuracy of approximation of the functions $\hat{h}_i(t)$ $(i = 1, 2, 3)$ and the spacecraft attitude motion relative to system $X_1X_2X_3$. Each figure is divided naturally into three parts — left-hand, middle and right-hand. The right-hand parts illustrate the quality of approximation of the functions $\hat{h}_i(t) - \Delta_i$ by the functions $h_i(t)$ used in (2). Here, solid lines present plots of $h_i(t)$ in the interval $t_0 \le t \le t_0 + T$; marks indicate the points $\big(t_0 + ns, \hat{h}_i(t_0 + ns) - \Delta_i\big)$, $n = 0, 1, \ldots, N$. The middle parts of the figures contain the plots of the angular rates $\omega_i(t)$. There are two plots in each coordinate system. The plots, obtained by minimization of (2), are depicted by lines without marks. The left-hand sides of the figures contain the plots of time dependence of the angles γ, δ, and β. They describe the motion of the system $z_1z_2z_3$ with respect to the system $X_1X_2X_3$. There are again two plots in each coordinate system. The lines without marks depict the plots obtained by minimization of (2).

These examples demonstrate the worse accuracy of approximation of the processed data than it was obtained in [1]. Here the values of σ_H are about two or three times greater than in [1]. Nevertheless the accuracy obtained is quite enough for our purposes. The standard deviations of initial angles $\gamma_g(t_0)$, $\delta_g(t_0)$, $\beta_g(t_0)$ are about 1.5° in the given examples; standard deviations of the angular rates $\Omega = \omega_1(t_0)$, $w_2(t_0) = \omega_2(t_0)$, $w_3(t_0) = \omega_3(t_0)$ are here about 0.0040 deg./s. The mechanical interpretation of the found motion one can find in [1].

8. Statistical technique of reconstruction of *Foton M-3* attitude motion by acceleration measurements. To reconstruct the spacecraft attitude motion by TAS3 measurement data we use at bottom the same technique as in

Sections 2, 6. The technique uses the functions $B_i(t)$ $(i = 1, 2, 3)$, constructed in Section 4, as a source information. It doesn't use them directly but deal with their values (see (4)) $B_i^{(n)} = B_i(t_n)$ $(n = 0, 1, \ldots, N)$. Recall that $\langle B_i \rangle = 0$.

Formula (1) allows to express vector components of a quasi-steady acceleration in system $x_1x_2x_3$ in terms of variables of equations (7) and coordinates of the point P. We assume that point is a location of TAS3. Then we can derive from (1) idealized calculation analogs for the functions $B_i(t)$ with correct mean values:

$$b_i = b_{ai} + \sum_{j=1}^{3} c_{ij}x_j\,, \quad b_{ai} = c\rho_a v u_i \quad (i = 1, 2, 3)\,, \tag{8}$$

$$c_{11} = \omega_2^2 + \omega_3^2 + \frac{\mu_e}{R^3}(3\gamma_1^2 - 1)\,, \quad c_{23} = \dot\omega_1 - \omega_2\omega_3 + \frac{3\mu_e}{R^3}\gamma_2\gamma_3\,,$$

$$c_{32} = -\dot\omega_1 - \omega_3\omega_2 + \frac{3\mu_e}{R^3}\gamma_3\gamma_2\,, \quad \text{etc.}\,,$$

$$u_1 = v_1\,, \quad u_2 = v_2\cos\varphi + v_3\sin\varphi\,, \quad u_3 = v_3\cos\varphi - v_2\sin\varphi\,,$$

$$\gamma_1 = \frac{z_1}{R}\,, \quad \gamma_2 = \frac{z_2\cos\varphi + z_3\sin\varphi}{R}\,, \quad \gamma_3 = \frac{z_3\cos\varphi - z_2\sin\varphi}{R}\,.$$

Here, x_j are the coordinates of the point P in the system $x_1x_2x_3$; one has to use substitution of indices $1 \to 2 \to 3 \to 1$ in order to obtain the other c_{ij}.

Formulas (8) don't take into account the influence of the Earth magnetic field on the TAS3 data as well as infra low-frequency errors in them. We considered these influence and errors in Section 4. We adopt models [4, 6] for their representation and write out the relations:

$$B_i(t) \approx \Delta_{bi} + \hat B_i(t, \tau) \quad (i = 1, 2, 3)\,,$$

$$\hat B_i(t, \tau) = b_i(t + \tau) + \sum_{j=1}^{3} m_{ij}h_j(t + \tau) + Z_i(t)\,, \tag{9}$$

$$Z_i(t) = A_{i0}(t - t_0) + \sum_{k=1}^{K} A_{ik}\sin\frac{\pi k(t - t_0)}{N\delta t}\,.$$

Here, Δ_{bi}, τ, m_{ij}, and A_{ik} are constant parameters; functions $b_i(t)$ and $h_i(t)$ are calculated along an appropriate solution of equations (7). As before, the initial point t_0 of the processed interval coincides with the instant t_0 in (7). The sense of some terms in (9) are following (see Section 4). The terms with $h_i(t)$ characterize the influence of the Earth magnetic field on the measurements; the terms $\Delta_{bi} + Z_i(t)$ compensate infra low-frequency errors (including erroneous constant biases) in the measurements. The number K must not be large in order to the frequency $K/2N\delta t$ is less than significant frequencies of functions (8).

We try to fit relations (9) by the least squares method and consider the functional

$$\Phi_b = \sum_{i=1}^{3} \left\{ \sum_{n=0}^{N} \Big[B_i^{(n)} - \hat{B}_i(t_n, \tau) \Big]^2 - (N+1)\Delta_{bi}^2 \right\}, \qquad (10)$$

$$\Delta_{bi} = \frac{1}{N+1} \sum_{n=0}^{N} \Big[B_i^{(n)} - \hat{B}_i(t_n, \tau) \Big].$$

It is obtained by transformation of the standard functional of least squares method that arises at fitting relations (9) for the points $t = t_n$. We minimize the functional over initial conditions of a solution of equations (7) at the point t_0 and the parameters p, m, ε, τ, c, x_i , m_{ij} , A_{ik} . There are $26 + 3K$ parameters in aggregate. Variation of c in the minimizing process is realized as variation of the dimensionless ratio $\chi = c/c_0$, where c_0 is the value of ballistic coefficient used in the subsystem of the spacecraft orbital motion (the motion of the point O).

We treat functional (10) in the following way. We join $25 + 3K$ of its arguments except τ in the vector z and consider (10) as the function $\Phi_b(z, \tau)$. The minimization of $\Phi_b(z, \tau)$ over z and τ is reduced to calculating the function

$$\hat{\Phi}_b(\tau) = \min_z \Phi_b(z, \tau)$$

at a sequence of points τ_n ($n = 1, 2, \dots$), which converges to the limit $\tau_* = \operatorname{argmin} \hat{\Phi}_b(\tau)$. We minimize $\Phi_b(z, \tau)$ over z, when τ is fixed, by Gauss–Newton's method. The quantities τ_* and $z_* = \operatorname{argmin} \Phi_b(z, \tau_*)$ are desired estimates of τ and z. We separate τ from the complete set of arguments of function (10) to simplify a preparation of the computer code for minimizing $\Phi_b(z, \tau)$. We take $\tau_1 = 0$ and use design values of x_i, $\chi = 1$, $m_{ij} = 0$, and results of processing magnetic measurements in the same interval $t_0 \le t \le t_N$ as an initial approximation to the minimum point of $\Phi_b(z, 0)$ in case of $Z_i(t) \equiv 0$ $(i = 1, 2, 3)$. Then we pass to case of $Z_i(t) \neq 0$, etc.

We use appropriate standard deviations to characterize the accuracy of the approximation of filtered data and scattering in the estimates τ_*, z_*. The standard deviation σ_b of errors in the data $B_i^{(n)}$ and the standard deviation σ_τ of τ_* are calculated by the formulas

$$\sigma_b = \sqrt{\frac{\hat{\Phi}_b(\tau_*)}{3N - 3K - 26}}, \quad \sigma_\tau^2 = 2\sigma_b^2 \left[\frac{\partial^2 \hat{\Phi}_b(\tau_*)}{\partial \tau^2} \right]^{-1}.$$

We evaluate the second derivative $\partial^2 \hat{\Phi}_b(\tau_*)/\partial \tau^2$ by difference approximation.

Standard deviations of the components of z_* are calculated under assumption that $\tau = \tau_*$ is known exactly, i.e., we use conditional standard deviations. We find

them in the following way. Let C be the matrix of normal equations, which appear at minimizing $\Phi_b(z, \tau_*)$ over z by Gauss-Newton's method; at that C is calculated at the point z_* and $2C \approx \partial^2\Phi_b(z_*, \tau_*)/\partial z^2$. The conditional standard deviations of the components of z_* are equal to the square roots of corresponding diagonal elements of the matrix $\sigma_b^2 C^{-1}$. We denote the conditional standard deviations of the quantities p, x_i, m_{ij} by σ_p , σ_{xi} , σ_{mij} , etc.

9. Real attitude motion of *Foton M-3* **(continuation).** The accelerometer TAS3 operated during the whole flight as well as the magnetometers. So we can reconstruct the spacecraft motion by two ways. An acceleration and a strength of a magnetic field have quite different physical nature. Therefore we estimate the coordination of measurement data of these quantities by comparing the spacecraft motions reconstructed in both ways above. This comparison was made for 5 time intervals listed in Table 1. Table 2 and Figs. 4 — 8 contain the results of processing the acceleration data in those intervals at $K = 5$. Table 2 contains some fitted parameters minimizing functional (10) and appropriate conditional standard deviations. Interval 1 was processed at $\lambda = 0.286$; the others intervals were processed at $\lambda = 0.255$.

Plots in the left-hand and right-hand parts of Figs. 4b, 5b, ..., 8b illustrate the accuracy of approximation of the filtered data by their calculated analogs. The left-hand parts contain the plots of the functions $\Delta_{bi} + \hat{B}_i(t, \tau)$. They are depicted by solid lines. The marks near these plots show the filtered data $\left(t_n + \tau, B_i^{(n)}\right)$, $n = 0, 1, \ldots, N$. The right-hand parts of the figures contain the plots of the residuals $e_i^{(n)} = B_i^{(n)} - \hat{B}_i(t_n, \tau) - \Delta_{bi}$ $(n = 0, 1, \ldots N;\ \ i = 1, 2, 3)$. These plots are the broken lines with vertexes in the points $\left(t_n + \tau, e_i^{(n)}\right)$. The standard deviation σ_b is a quantitative characteristic of the approximation accuracy. Its values are given in figure captions and in Table 2. These values are small nevertheless they are about two times greater than in [3] and Section 4. This is no surprise because we used there another way of constructing the calculated analog of the functions $B_i(t)$. The figures and the values of σ_b in Table 2 demonstrate that the correction for the magnetic field and the elimination of infra low-frequency errors allow to coordinate acceleration measurement data and their calculated analog rather exactly.

The middle parts of Figs. 4b, 5b, ..., 8b contain the plots of functions (8). The plots illustrate the real quasi-steady accelerations near the point of TAS3 location.

The marked plots in the left-hand and middle parts of Figs. 4a, ..., 8a describe the spacecraft attitude motion relative to the system $X_1X_2X_3$. These plots are defined at $\tau \le t - t_0 \le T + \tau$. One can compare the plots with marks and without them in the figures and feel that spacecraft motions, found in both above ways, coincide sufficiently well. Some discrepancies in the plots of the angles γ and δ are caused by shifts on 360°. They are not significant. Figs. 4c,..., 8c confirm that; they

contain the plots of the quantities a_{i1} and a_{2i} $(i = 1, 2, 3)$. The quantities a_{i1} are the components of the axis z_1 unit vector in the system $X_1X_2X_3$; the quantities a_{2i} are the components of the axis X_2 unit vector in the system $z_1z_2z_3$. These plots give exhaustive presentation of spacecraft motion in intervals of Table 2. We see in the figures that motion reconstructions of axis z_1, found by processing the measurement data of different types, coincide well. The coincidence is somewhat worse in case of the motion reconstructions of the axis X_2.

The found solutions have conditional standard deviations of the initial angles $\gamma(t_0)$, $\delta(t_0)$, $\beta(t_0)$ less than 2.1°; conditional standard deviations of the quantities Ω, $w_2(t_0)$, $w_3(t_0)$ are less than 0.0055 deg./s. These estimates are close to the estimates obtained by processing the magnetic measurements. The estimates of the parameters p, m, ε and their standard deviations in Table 2 somewhat differ from the respective estimates in Table 1.

We can obtain some information about accuracy of our motion reconstruction comparing the estimates of c, τ, x_i, and m_{ij} found by the technique of Section 8 with analogous estimates found in other ways. The estimates of the ratio χ in Table 2 show that coefficient c in (8) are closed to the value of $c_0 \approx 0.0014$ m^2/kg that was obtained by smoothing two line elements. The estimates of x_i, τ, and m_{ij} in the table can be compared with the estimates mentioned in Section 4. Those estimates differ in a way from the estimates in Table 2. But the technique of Section 8 doesn't take into account that single-axis TAS3 sensors have certain shifts with respect to each other (taking the shifts into account doesn't increase the accuracy of the technique of Section 8). These shifts are about 50 mm. So we got a proper agreement in this case.

The standard deviations of the estimates of m_{ij} in Section 4 are about the same as in Table 2. Those estimates differ from estimates in Table 2 but are rather similar to them. The estimates of τ in Table 2 lie in the same range as estimates of this quantity in [3], but they have more large scattering.

The correction of TAS3 measurement data for the Earth magnetic field and the elimination of infra low-frequency errors allowed to achieve a good coincidence of spacecraft motions reconstructed in different ways. This good coincidence is not surprising because acceleration measurements contain certain information about the Earth magnetic field.

The use of expressions $Z_i(t)$ $(i = 1, 2, 3)$ with $K = 5$ in formulas (5) and (9) doesn't affect the frequencies above 0.00012 Hz in the comparison of the functions $B_i(t)$ and $b_i(t)$. Functions (8) and their analogues, used in Section 4, have frequencies less than 0.002 Hz for the considered motions of *Foton M-3* (compare [3]). These facts testify to the sufficiently high accuracy of the accelerometer TAS3 in the frequency range $0.0002 \div 0.002$ Hz.

This work was partly supported by Russian Foundation for Basic Research (project 08-01-00467).

References

1. Beuselinck T., Van Bavinchove C., Abrashkin V.I., Kazakova A.E., Sazonov V.V. Determination of the spacecraft *Foton M-3* attitude motion on measurements of the Earth magnetic field. Preprint, Keldysh Institute of Applied Mathematics, Russia Academy of Sciences, No. 80, 2008.
2. Sazonov V.V., Komarov M.M., Polezhaev V.I., Nikitin S.A., Ermakov M.K., Stazhkov V.M., Zykov S.G., Ryabukha S.B., Acevedo J., Liberman E. Microaccelerations on board the Mir orbital station and prompt analysis of gravitational sensitivity of convective processes of heat and mass transfer. Cosmic Research, 1999, vol. 37, No. 1, pp. 80-94.
3. Beuselinck T., Van Bavinchove C., Sazonov V.V., Chebukov S.Yu. An analysis of low-frequency component in microacceleration measurements made onboard *Foton M-2* satellite. Cosmic Research, 2008, vol. 46, No. 5, pp. 436-455.
4. Beuselinck T., Van Bavinchove C., Sazonov V.V., Chebukov S.Yu. Determination of *Foton M-2* satellite attitude motion by the data of microacceleration measurements. Cosmic Research, 2009, vol. 47, No. 6, pp. 500-512.
5. GOST R (State standard) 25645.166-2004. Earth upper atmosphere. Density model for ballistic support of flights of artificial Earth satellites. Moscow, 2004.
6. Sazonov V.V. Processing angular rate and acceleration measurements obtained onboard the spacecraft *Foton-12*. Preprint, Keldysh Institute of Applied Mathematics, Russia Academy of Sciences, No. 62, 2008.

Table 1. Results of processing the magnetic field measurements.

Interval (date)	t_0 UTC	s_H (g)	p	s_p	m	s_m	e	s_e
			10^{-5} m/kg		10^{-7} Oe^{-1}s^{-2}		10^{-9} s^{-2}	
1 (19)	08:55:40	3053	–13.4	1.7	–0.81	0.13	0.3	0.43
2 (21)	08:42:24	1657	–8.9	0.61	2.31	0.14	4.4	0.25
3 (23)	07:09:05	2685	–2.0	1.4	0.46	0.26	1.3	0.33
4 (24)	05:19:05	3098	–13.5	2.2	3.61	0.39	7.9	0.42
5 (24)	19:12:27	4600	27.7	2.1	2.22	0.54	40.1	0.55

Table 2. Results of processing the acceleration measurements. The unit of m_{ij} and s_{mij} is 10^{-7} m/(s^2·Oe).

Interval	s_b (10^{-6} m/s^2)	t (s)	s_t (s)	p	s_p	m	s_m	e	s_e	c	s_c
				10^{-5} m/kg		10^{-7} Oe^{-1}s^{-2}		10^{-9} s^{-2}			
1	1.196	39	7.2	–17.5	2.0	–1.64	0.20	–0.84	0.46	0.930	0.038
2	0.883	51	4.6	–7.4	0.90	–2.64	0.20	2.73	0.28	0.987	0.022
3	1.422	86	8.0	–33.0	1.9	–1.08	0.46	2.14	0.37	0.806	0.032
4	1.504	31	9.8	–8.3	2.5	4.51	0.60	9.06	0.46	0.871	0.034
5	1.482	–1	8.8	–7.5	2.1	13.0	0.41	50.9	0.53	0.962	0.032

Interval	x_1 (mm)	s_{x1} (mm)	x_2 (mm)	s_{x2} (mm)	x_3 (mm)	s_{x3} (mm)	m_{11}	s_{m11}	m_{12}	s_{m12}	m_{13}	s_{m13}
1	124	12	–183	8.4	–301	5.7	–198	2.3	–126	4.8	–174	3.7
2	103	5.8	–185	4.6	–302	3.0	–187	1.6	–123	3.0	–181	2.3
3	170	9.0	–181	6.3	–287	4.2	–222	2.6	–130	4.3	–174	3.7
4	187	9.5	–186	6.9	–286	5.0	–221	3.0	–124	5.0	–184	4.0
5	120	9.1	–228	7.6	–278	6.0	–217	3.1	–120	4.6	–162	3.8

Interval	m_{21}	s_{m21}	m_{22}	s_{m22}	m_{23}	s_{m23}	m_{31}	s_{m31}	m_{32}	s_{m32}	m_{33}	s_{m33}
1	3	2.3	–157	3.4	–100	4.3	–27	2.2	–57	4.3	–154	2.6
2	18	1.5	–164	2.0	–104	2.7	–12	1.5	–57	2.5	–147	1.6
3	15	2.6	–159	3.3	–100	3.9	–13	2.6	–60	3.7	–142	2.7
4	2	2.7	–154	3.8	–99	4.2	–21	2.7	–64	4.0	–147	3.0
5	6	2.5	–157	3.0	–91	4.5	–13	2.6	–61	4.0	–131	3.1

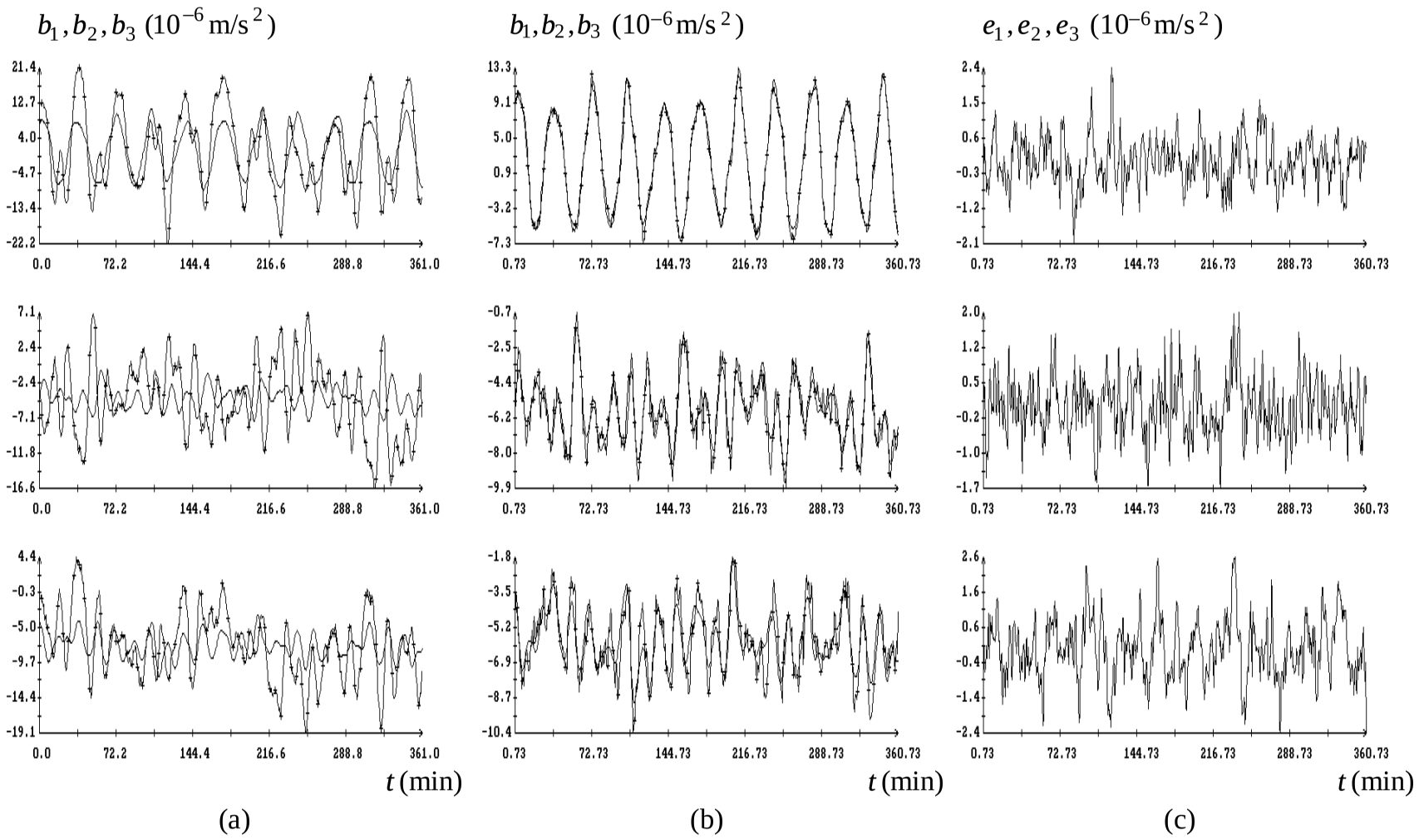

Fig. 1. The accelerations at the point of TAS3 location; the instant $t = 0$ corresponds to 08:55:40 UTC 19.09.2007 (interval 10 in [1]); (a) the filtered data without corrections and their calculation analog; (b) the filtered data after corrections and the calculation analog, $s_b = 7.1 \cdot 10^{-7}$ m/s^2, $t = 19$ s, $s_t = 0.97$ s; (c) the errors of the approximation.

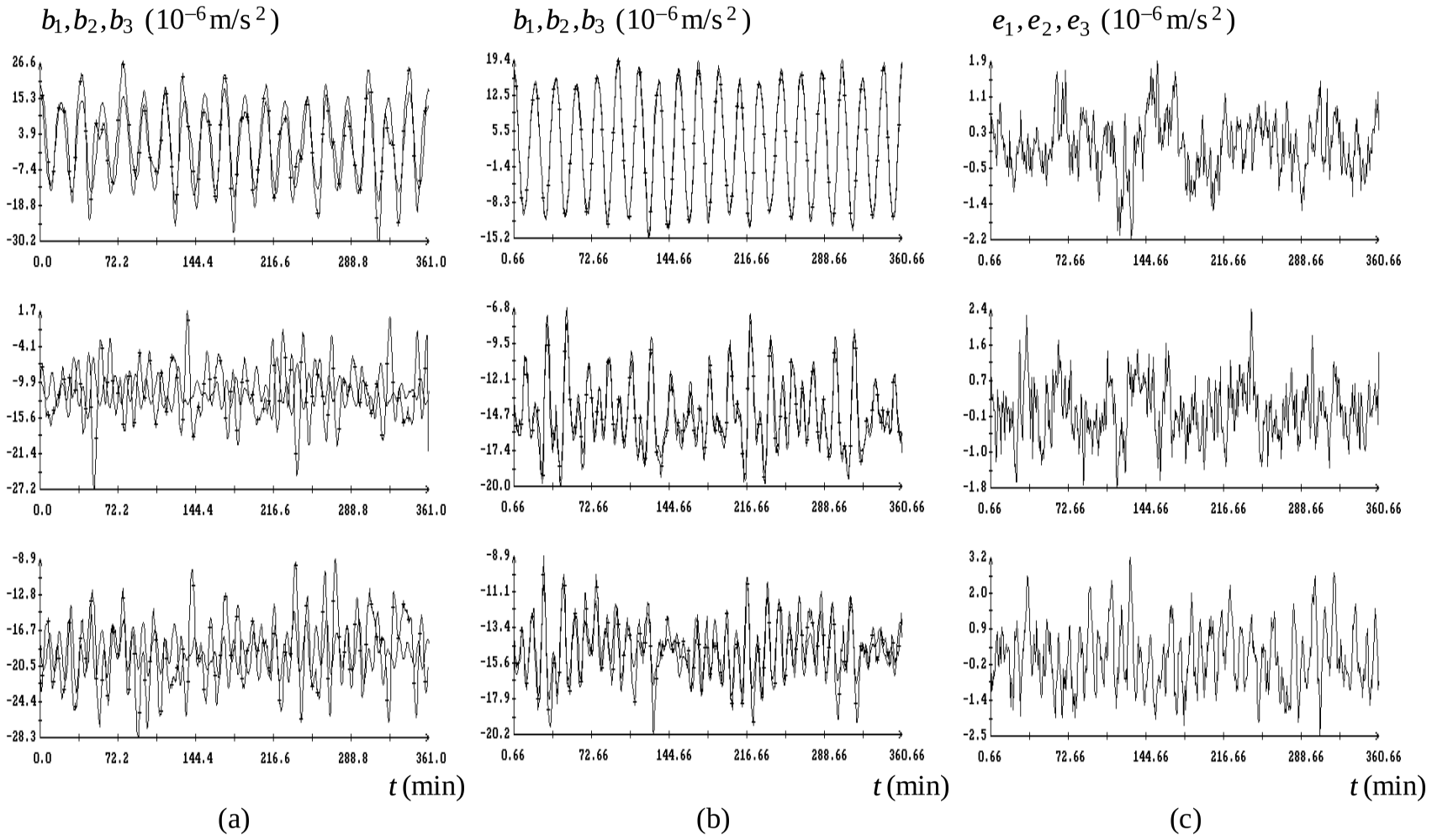

Fig. 2. The accelerations at the point of TAS3 location; the instant $t = 0$ corresponds to 07:09:05 UTC 23.09.2007 (interval 14 in [1]); (a) the filtered data without corrections and their calculation analog; (b) the filtered data after corrections and the calculation analog, $s_b = 8.1 \cdot 10^{-7}$ m/s^2, $t = 18$ s, $s_t = 0.90$ s; (c) the errors of the approximation.

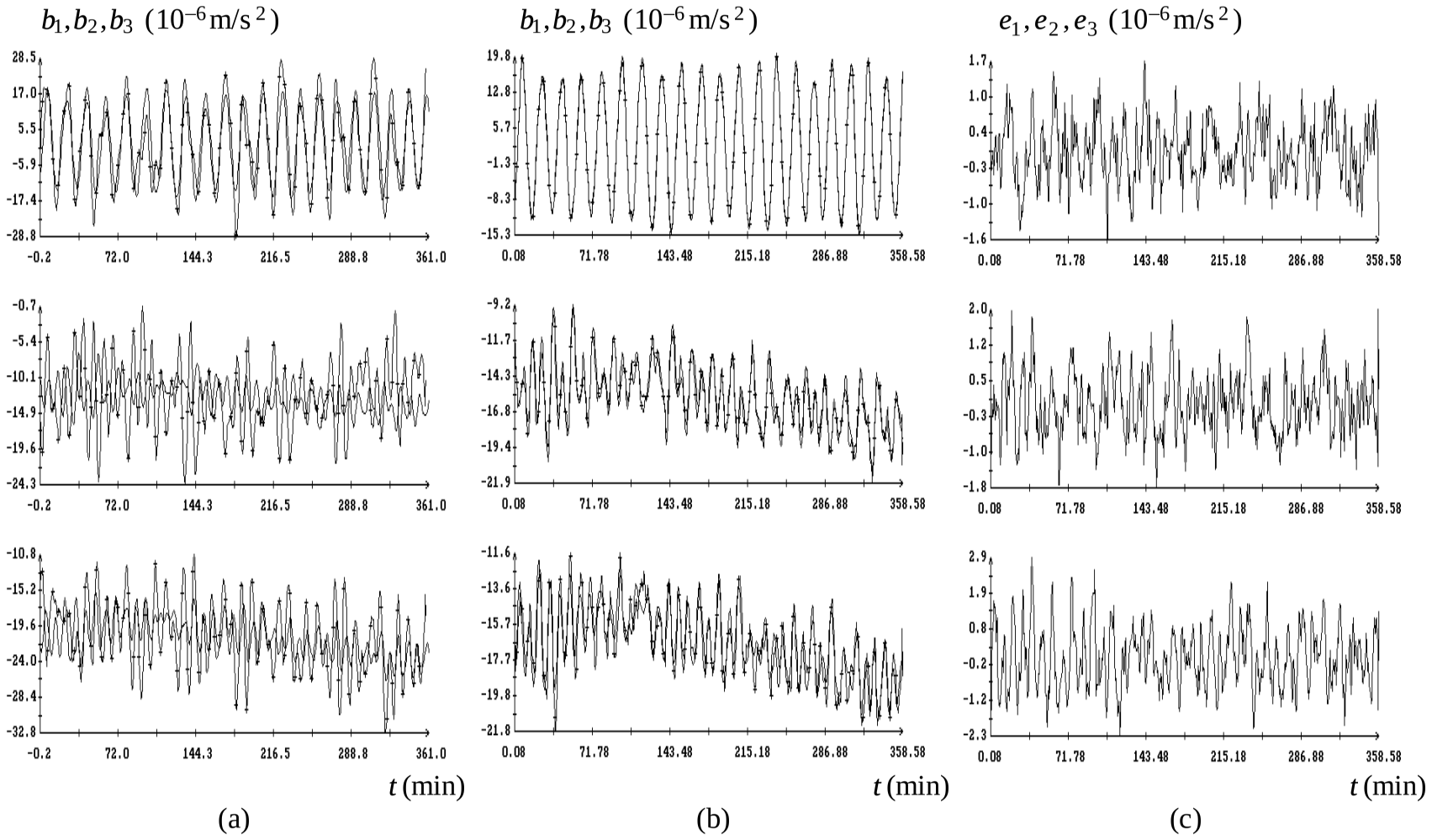

Fig. 3. The accelerations at the point of TAS3 location; the instant $t = 0$ corresponds to 19:12:27 UTC 24.09.2007 (interval 16 in [1]); (a) the filtered data without corrections and their calculation analog; (b) the filtered data after corrections and the calculation analog, $s_b = 7.4 \cdot 10^{-7}\,\mathrm{m/s^2}$, $t = 17\,\mathrm{s}$, $s_t = 0.80\,\mathrm{s}$; (c) the errors of the approximation.

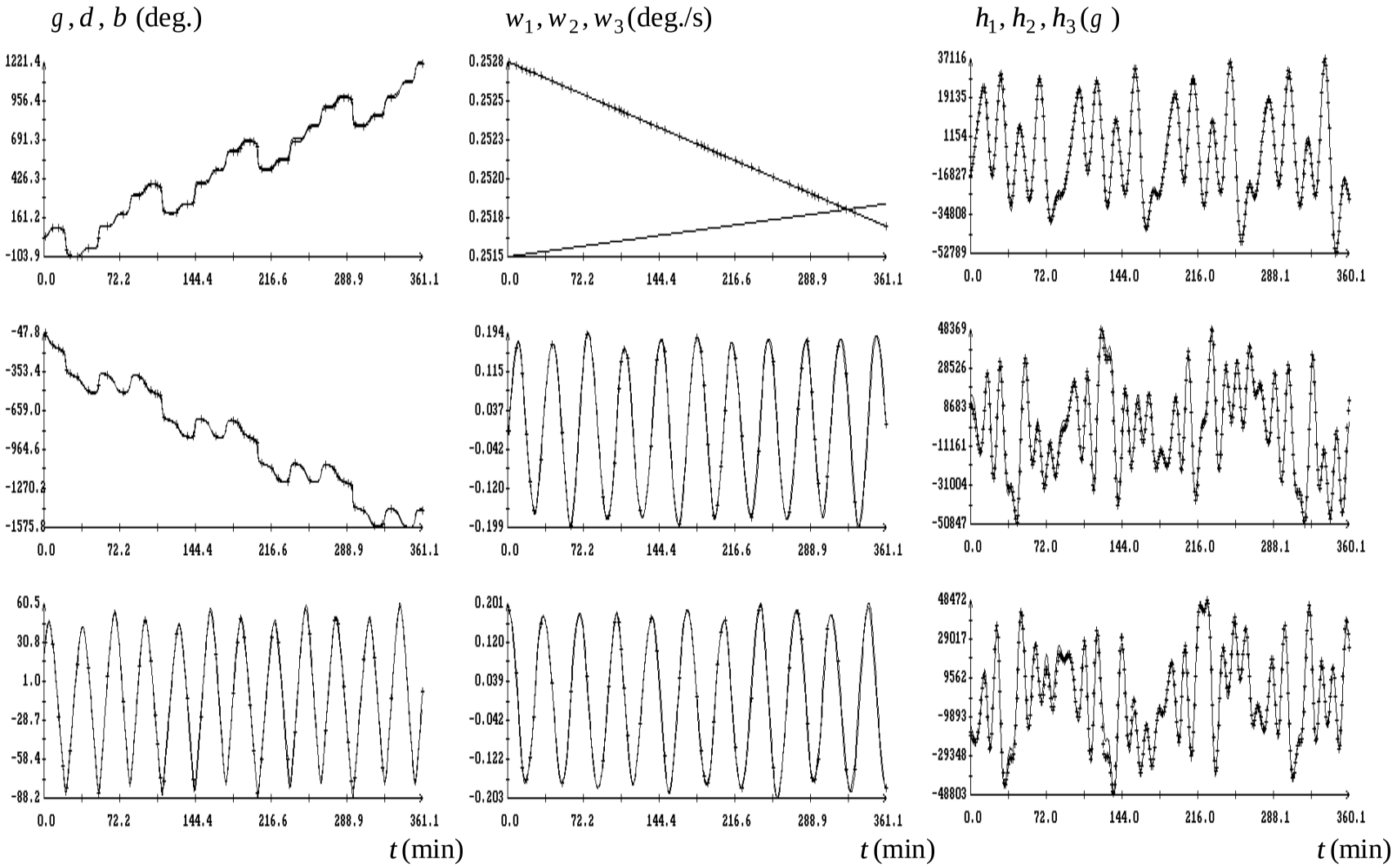

Fig. 4a. The instant $t = 0$ in the plots corresponds to 08:55:40 UTC 19.09.2007, $s_H = 3054\,g$.

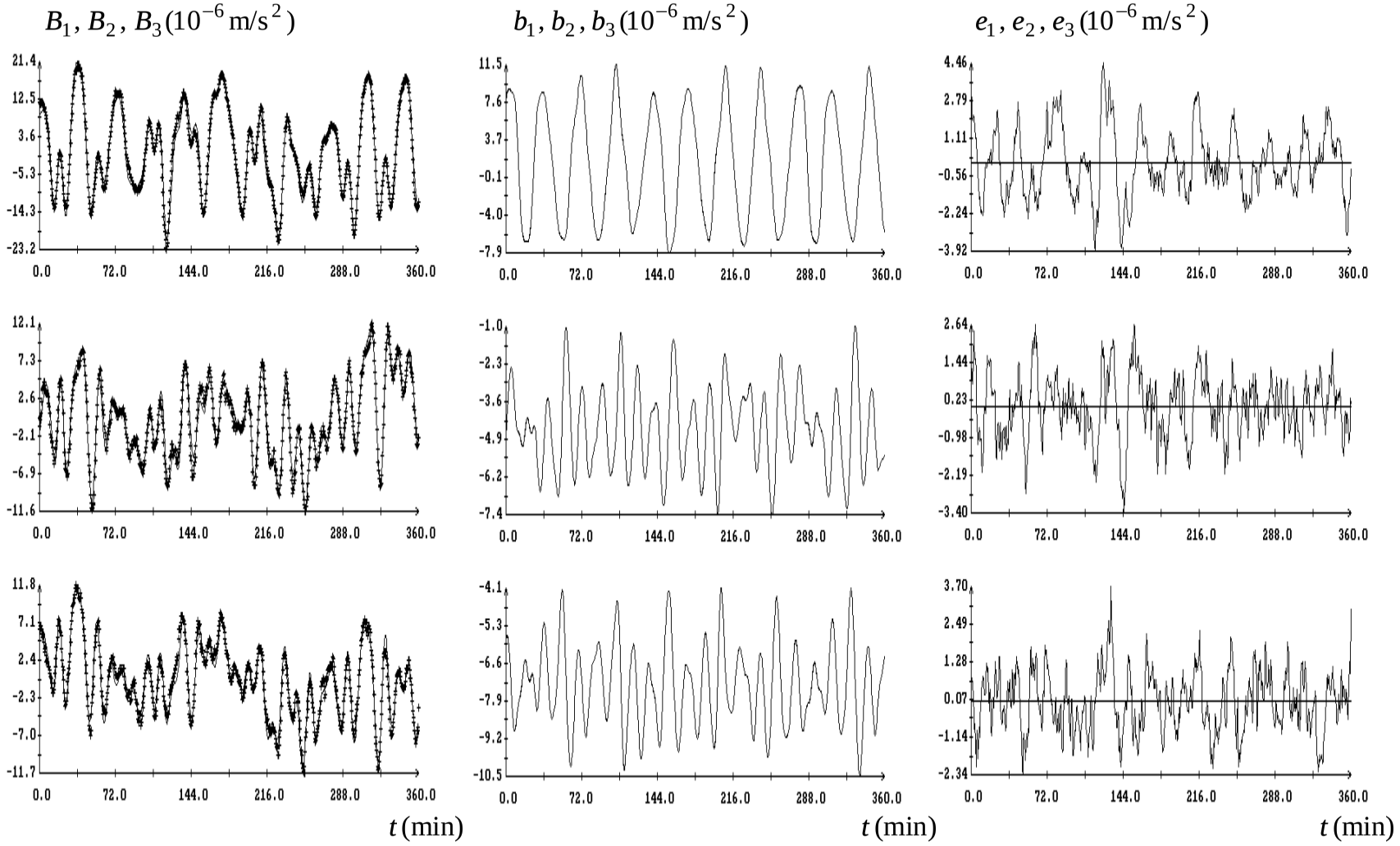

Fig. 4b. The instant $t = 0$ in the plots corresponds to $t_0 + t$, $t_0 =$ 08:56:05 UTC 19.09.2007, $t = 39\,\mathrm{s}$, $s_t = 7.2\,\mathrm{s}$, $s_b = 1.196 \cdot 10^{-6}\,\mathrm{m/s^2}$.

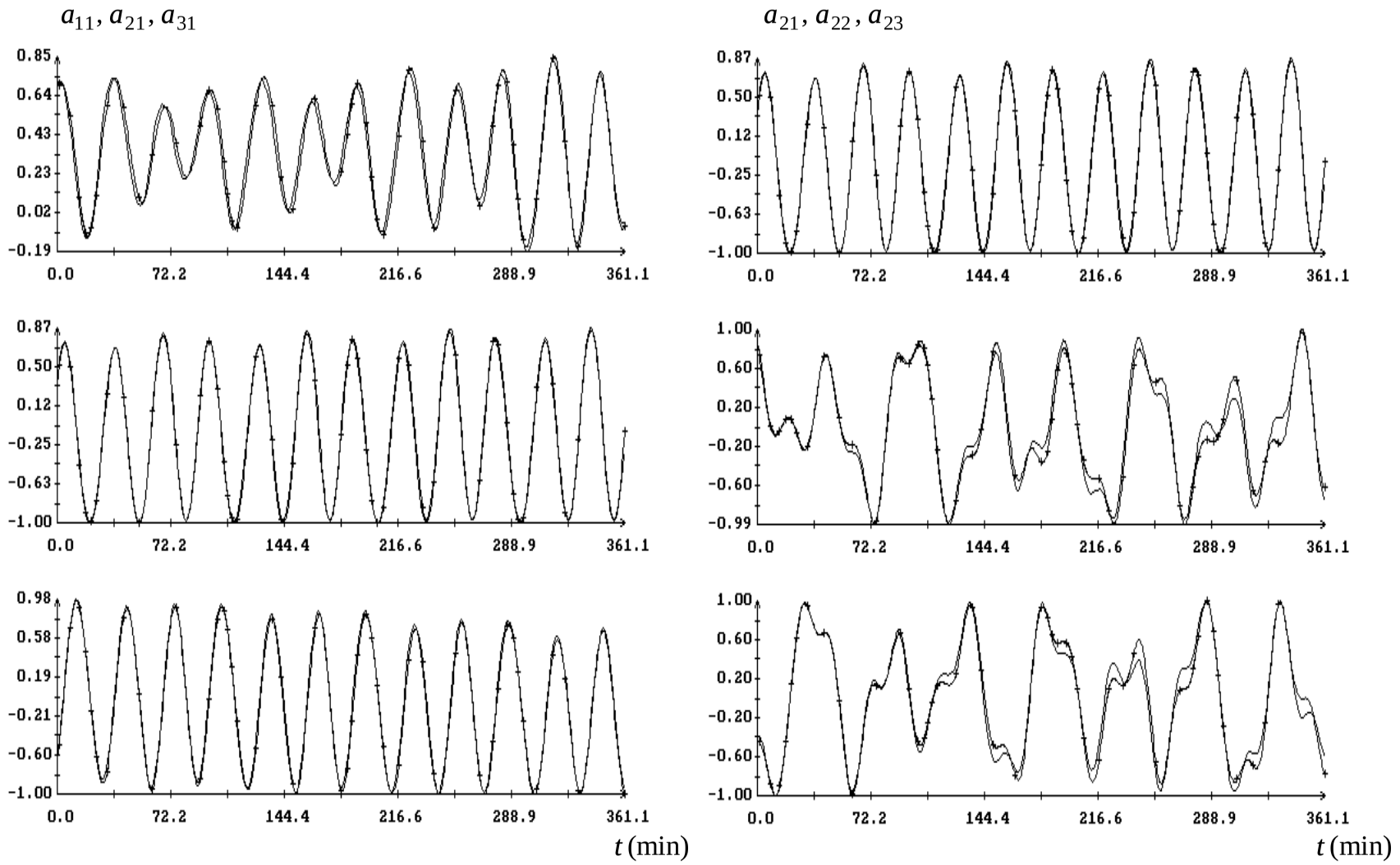

Fig. 4c. The instant $t = 0$ in the plots corresponds to $t_0 + t$, $t_0 =$ 08:56:05 UTC 19.09.2007, $t = 39$ s.

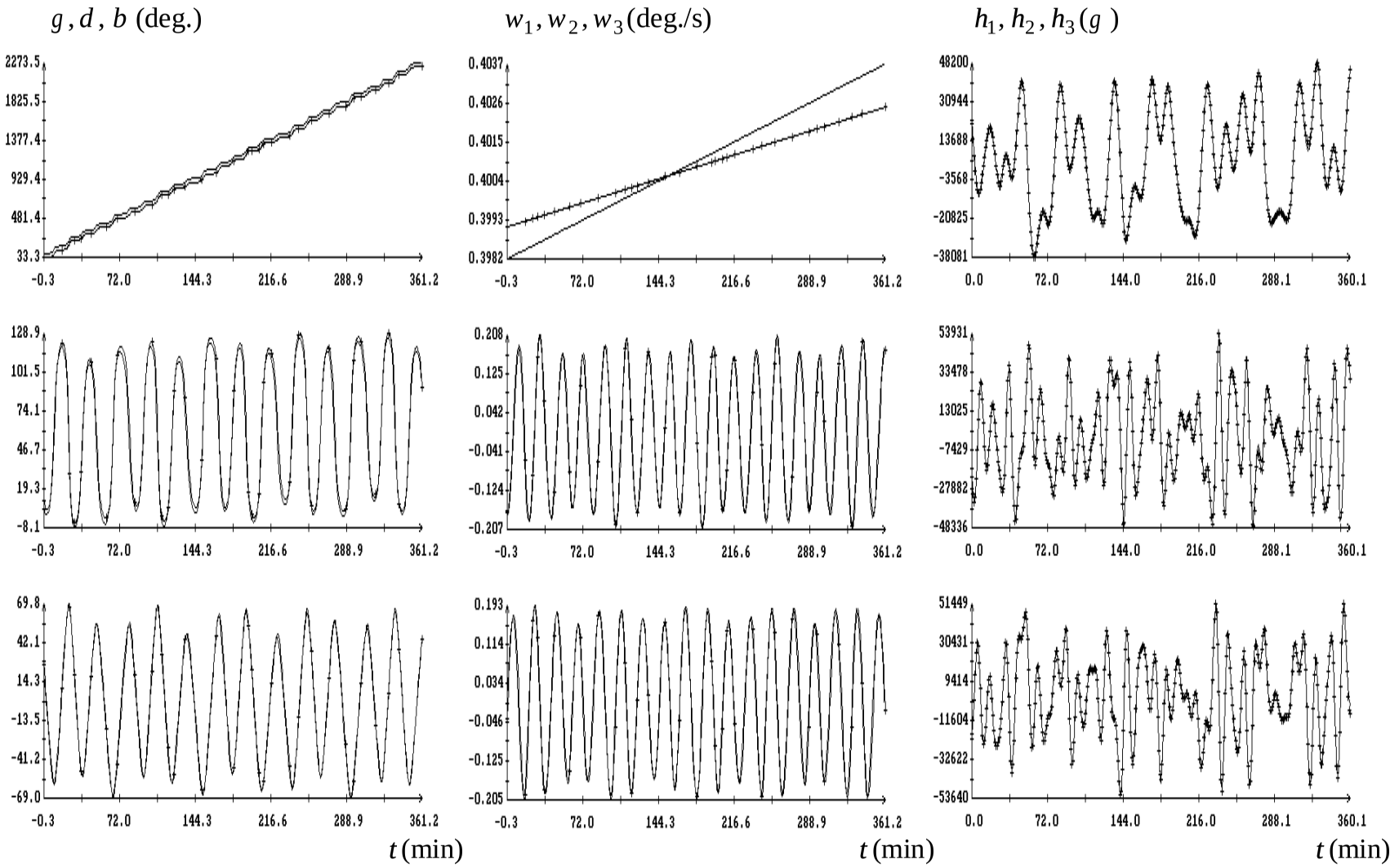

Fig. 5a. The instant $t = 0$ in the plots corresponds to 08:42:24 UTC 21.09.2007, $s_H = 1652\,g$.

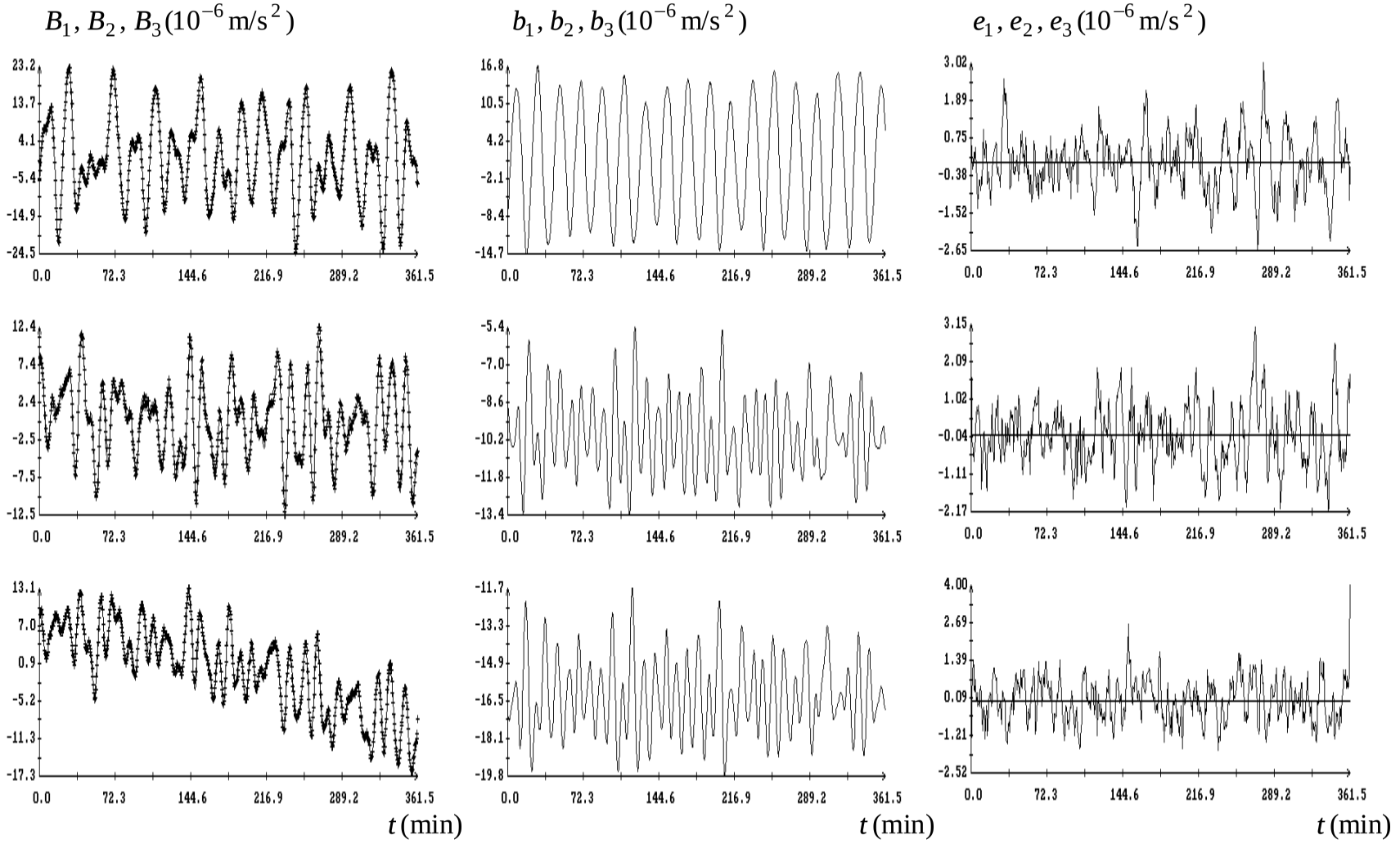

Fig. 5b. The instant $t = 0$ in the plots corresponds to $t_0 + t$, $t_0 =$ 08:41:14 UTC 21.09.2007, $t = 51\mathrm{s}$, $s_t = 4.6\,\mathrm{s}$, $s_b = 0.837 \cdot 10^{-6}\,\mathrm{m/s^2}$.

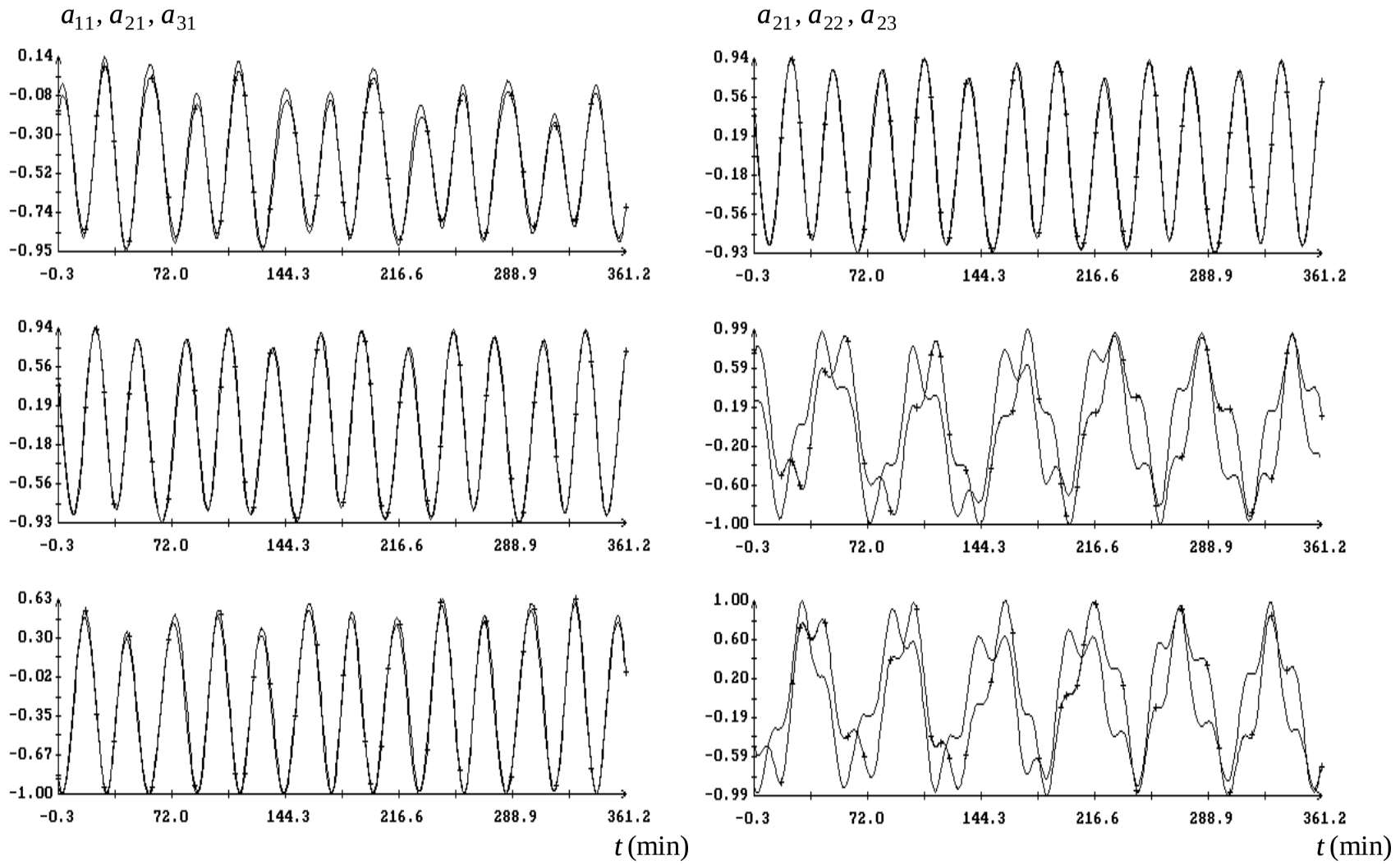

Fig. 5c. The instant $t = 0$ in the plots corresponds to $t_0 + t$, $t_0 =$ 08:41:14 UTC 21.09.2007, $t =$ 51s.

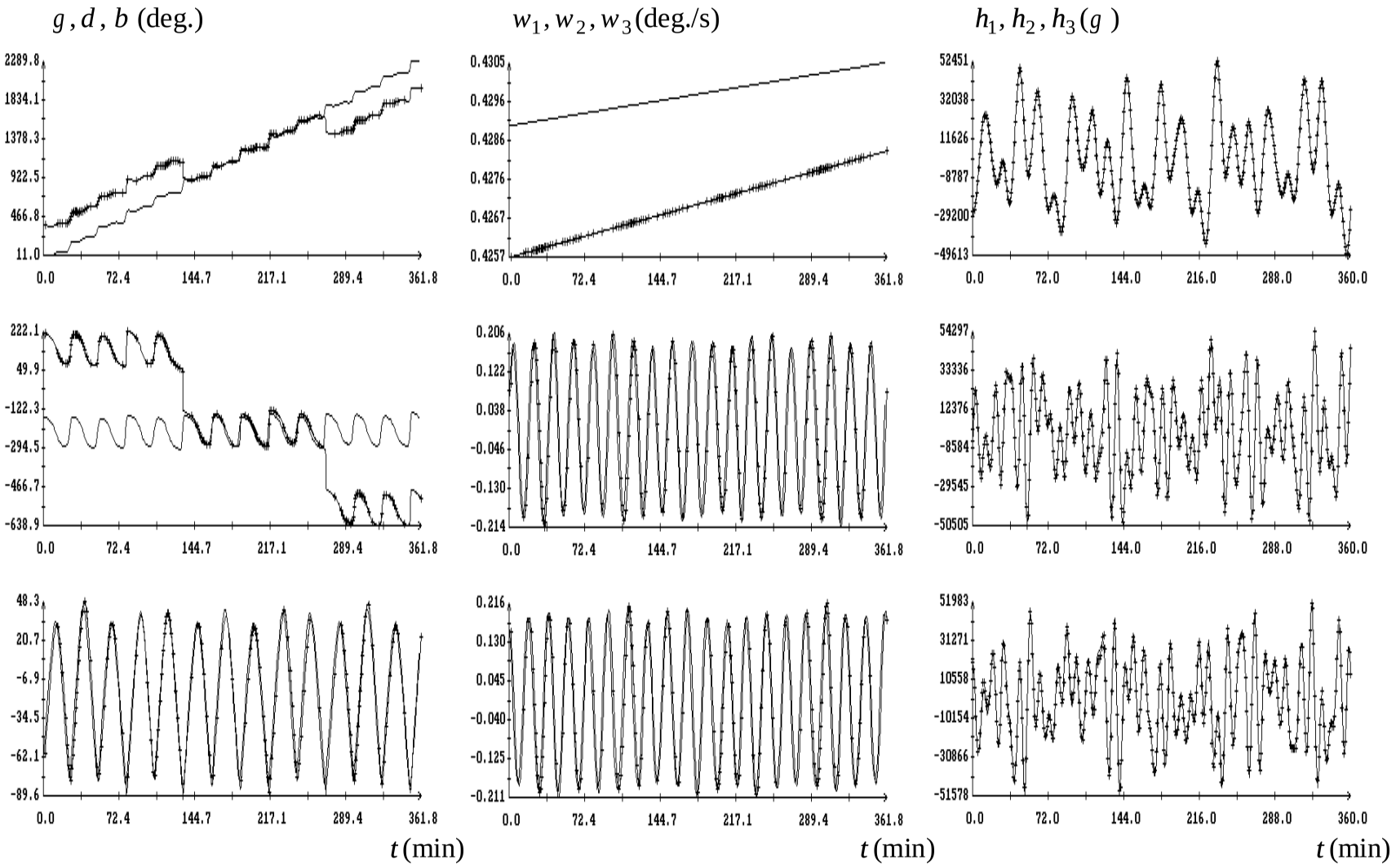

Fig. 6a. The instant $t = 0$ in the plots corresponds to 07:09:06 UTC 23.09.2007, $s_H = 2685\,g$.

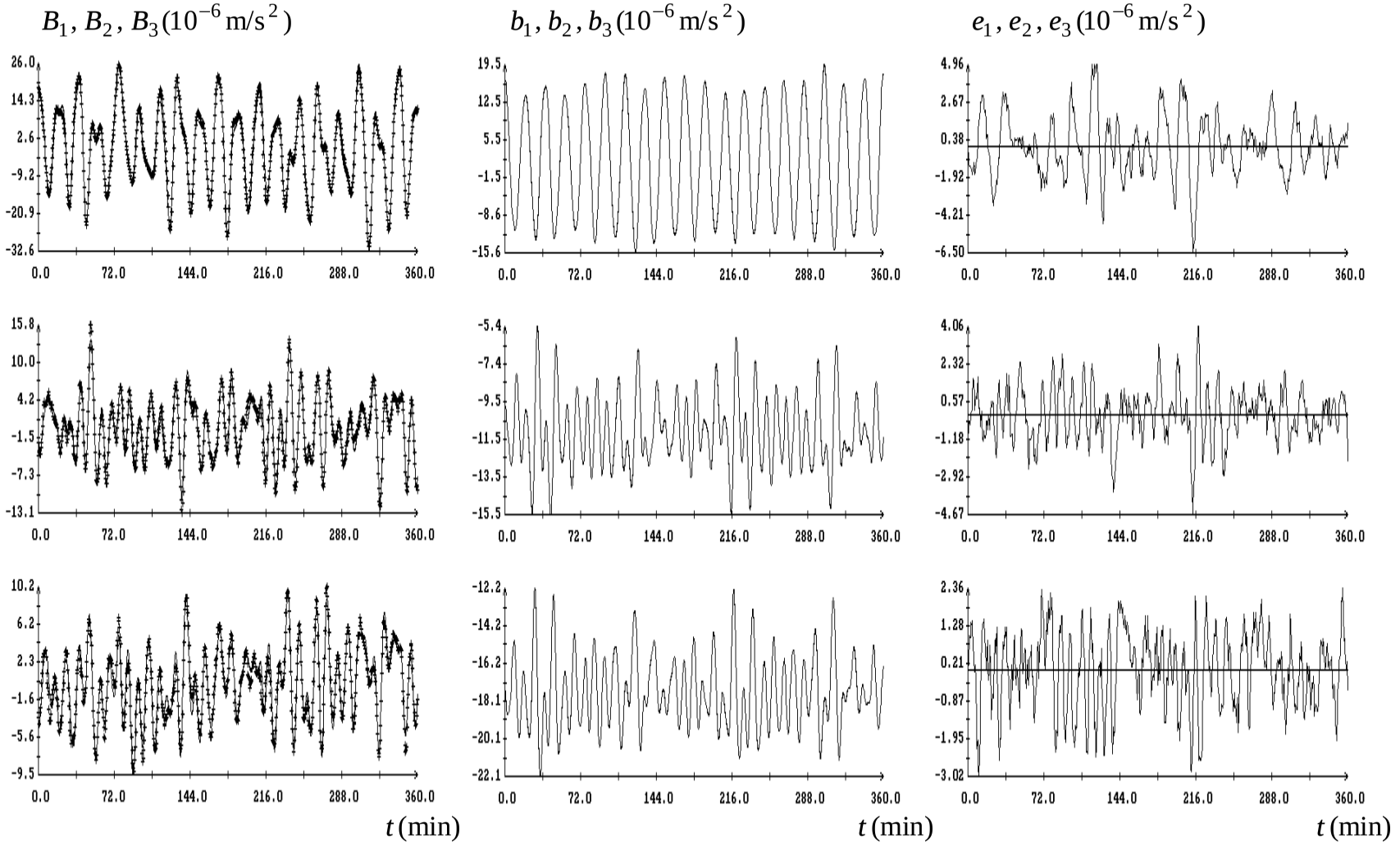

Fig. 6b. The instant $t = 0$ in the plots corresponds to $t_0 + t$, $t_0 =$ 07:09:27 UTC 23.09.2007, $t = 86\,\mathrm{s}$, $s_t = 8.0\,\mathrm{s}$, $s_b = 1.422 \cdot 10^{-6}\,\mathrm{m/s^2}$.

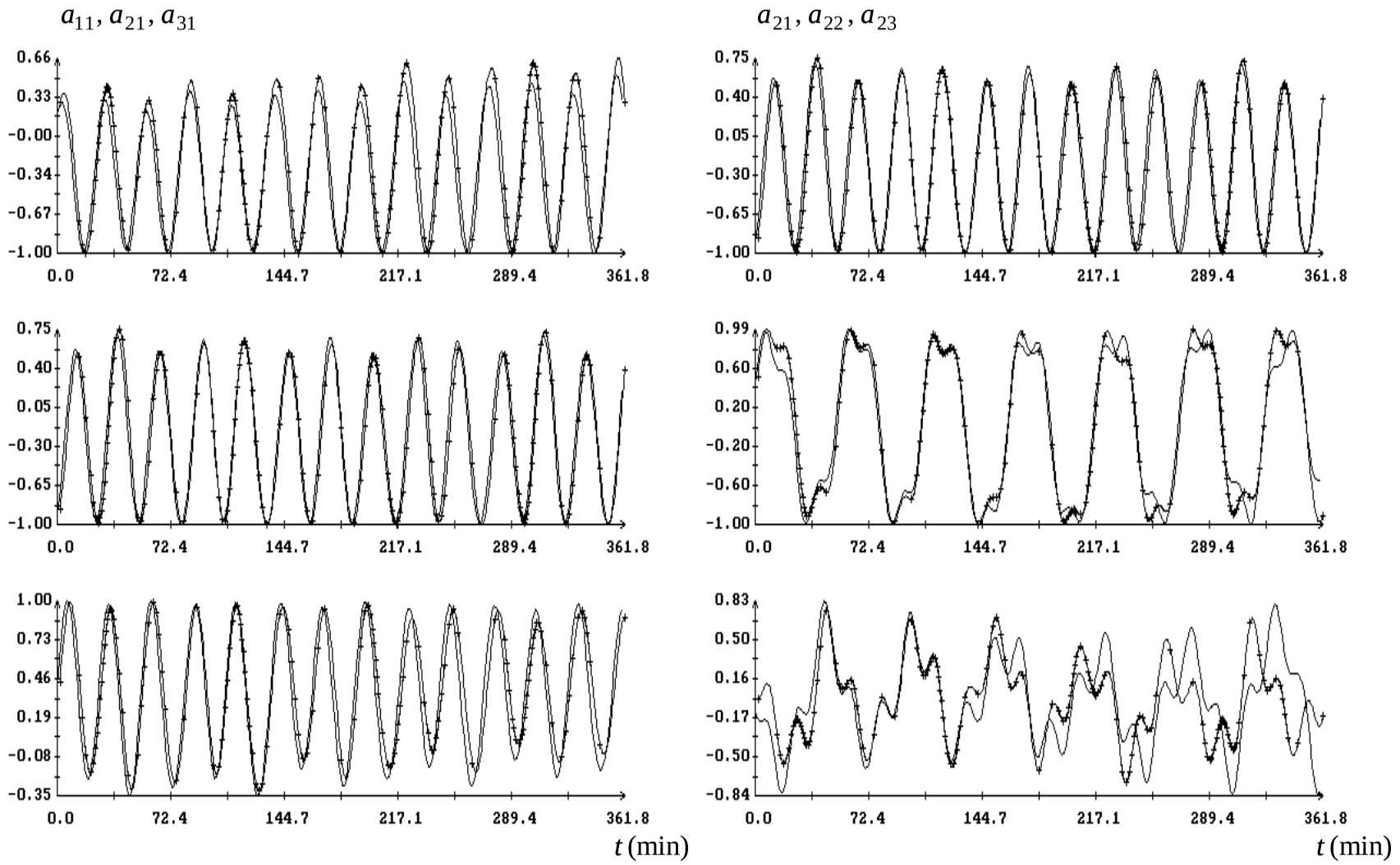

Fig. 6c. The instant $t = 0$ in the plots corresponds to $t_0 + t$, $t_0 =$07:09:27 UTC 23.09.2007, $t = 86$ s.

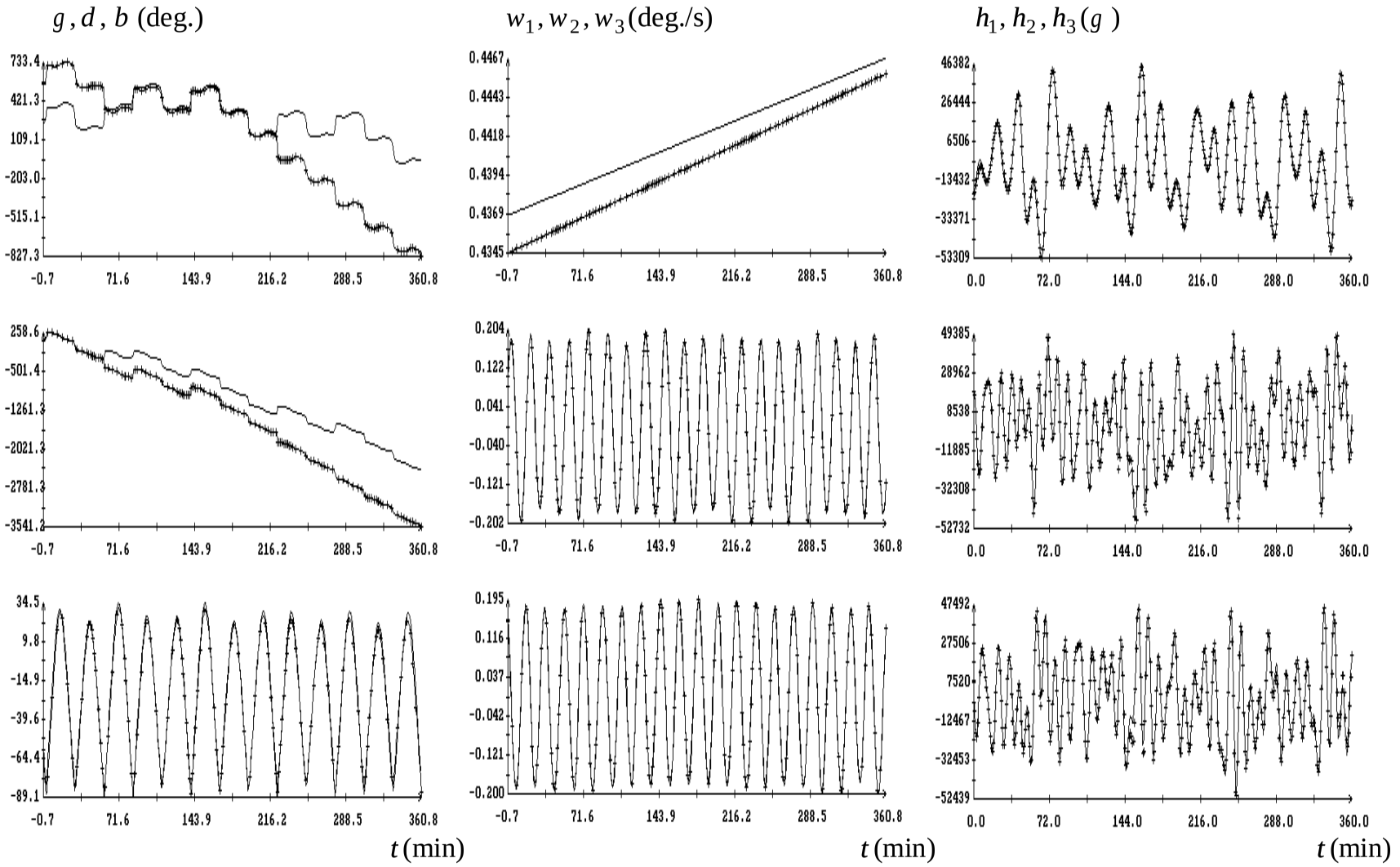

Fig. 7a. The instant $t = 0$ in the plots corresponds to 05:19:05 UTC 24.09.2007, $s_H = 3098\,g$.

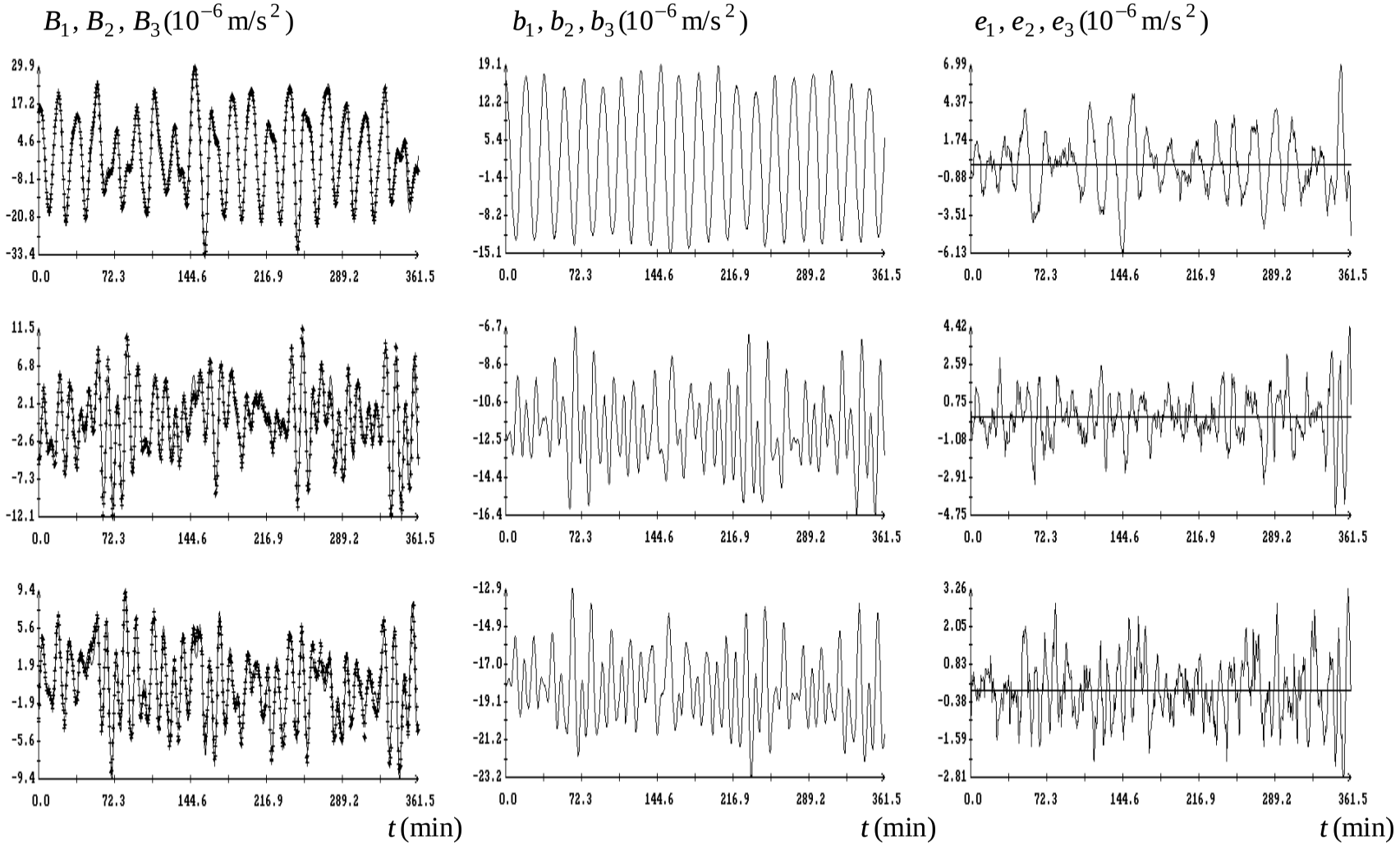

Fig. 7b. The instant $t = 0$ in the plots corresponds to $t_0 + t$, $t_0 =$ 05:17:54 UTC 24.09.2007, $t = 31\mathrm{s}$, $s_t = 9.8\,\mathrm{s}$, $s_b = 1.504 \cdot 10^{-6}\,\mathrm{m/s^2}$.

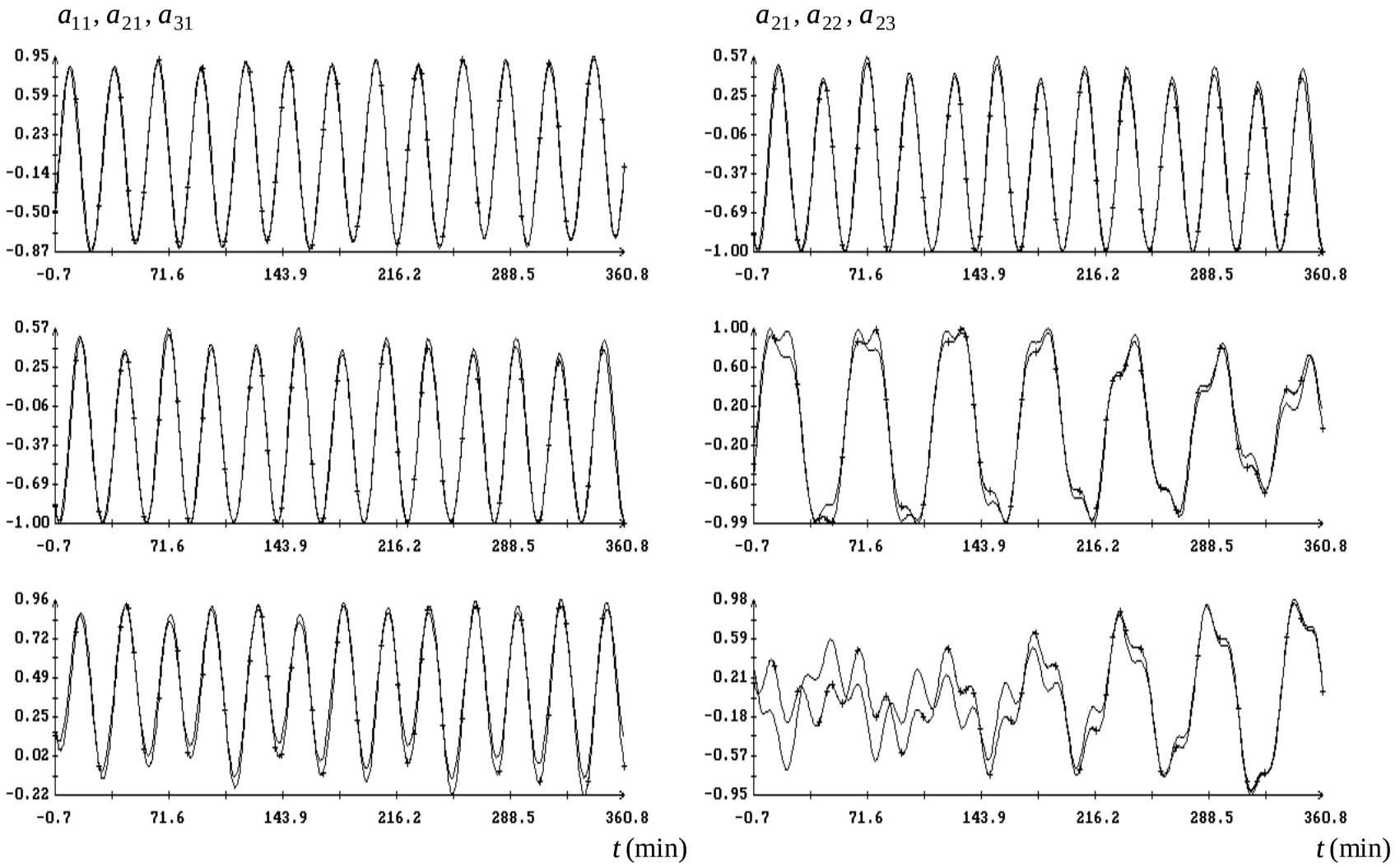

Fig. 7c. The instant $t = 0$ in the plots corresponds to $t_0 + t$, $t_0 =$ 05:17:54 UTC 24.09.2007, $t =$ 31s.

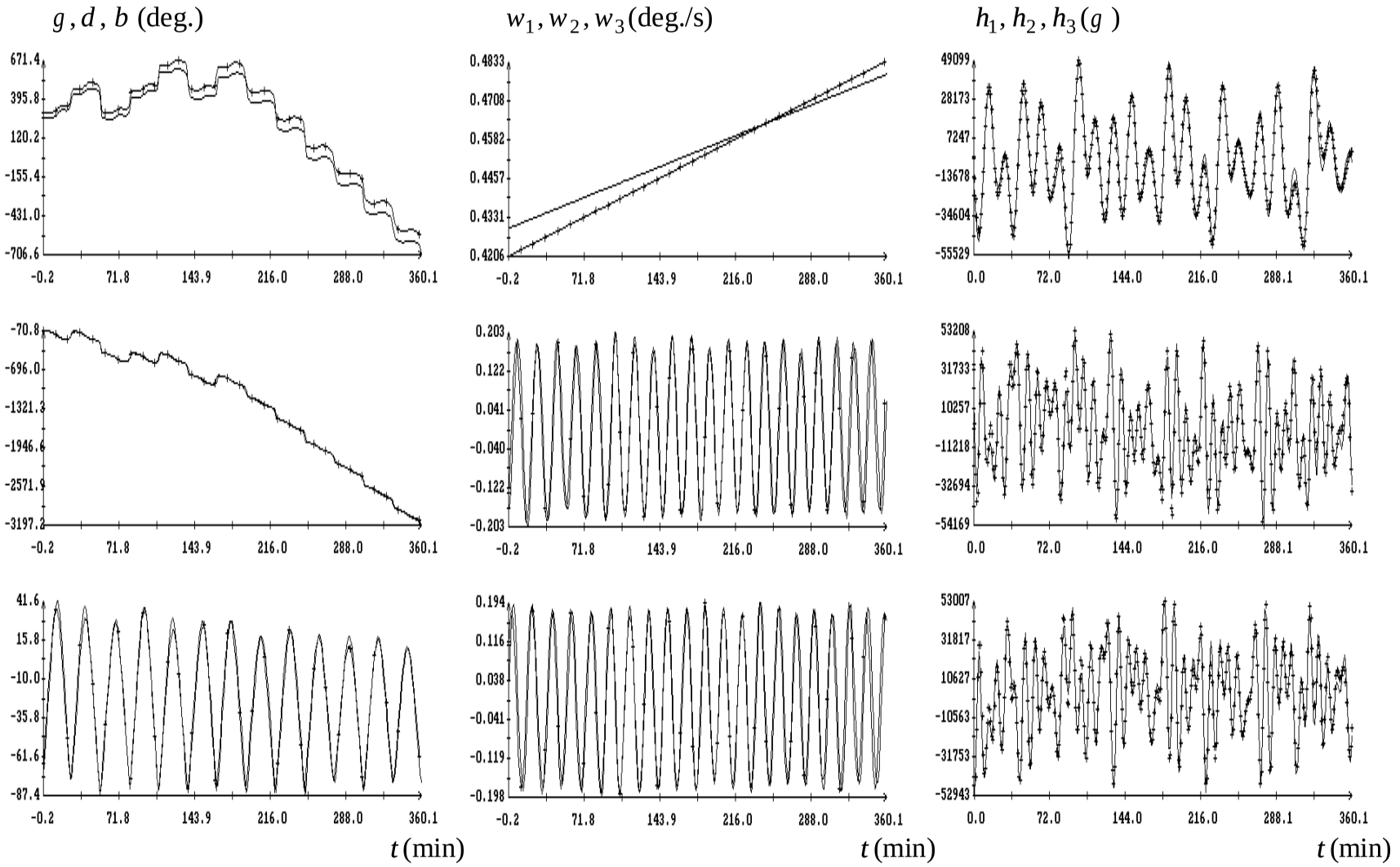

Fig. 8a. The instant $t = 0$ in the plots corresponds to 19:12:27 UTC 24.09.2007, $s_H = 4563\,g$.

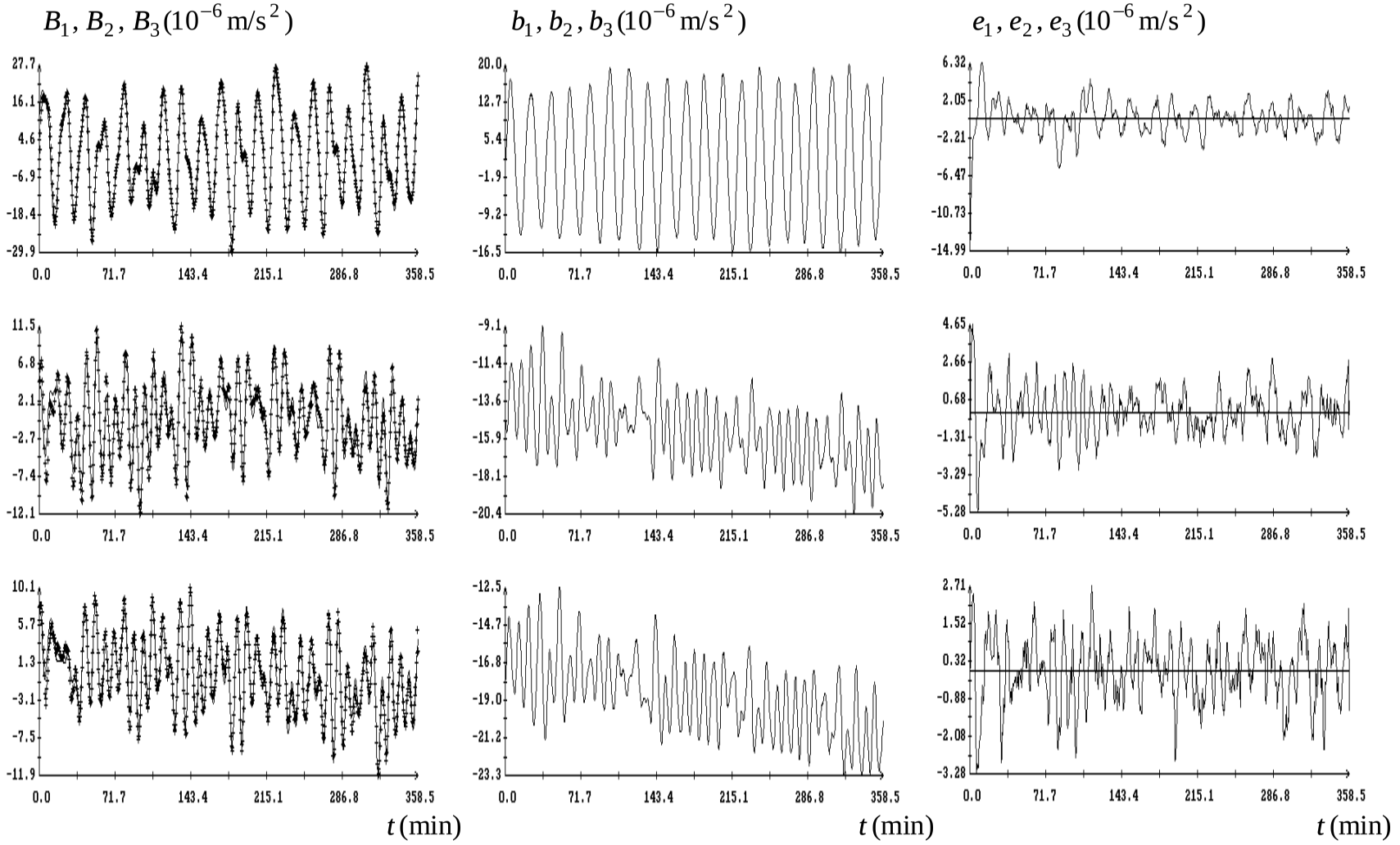

Fig. 8b. The instant $t = 0$ in the plots corresponds to $t_0 + t$, $t_0 =$ 19:12:15 UTC 24.09.2007, $t = -1$s, $s_t = 8.8$s, $s_b = 1.482 \cdot 10^{-6}\,\mathrm{m/s^2}$.

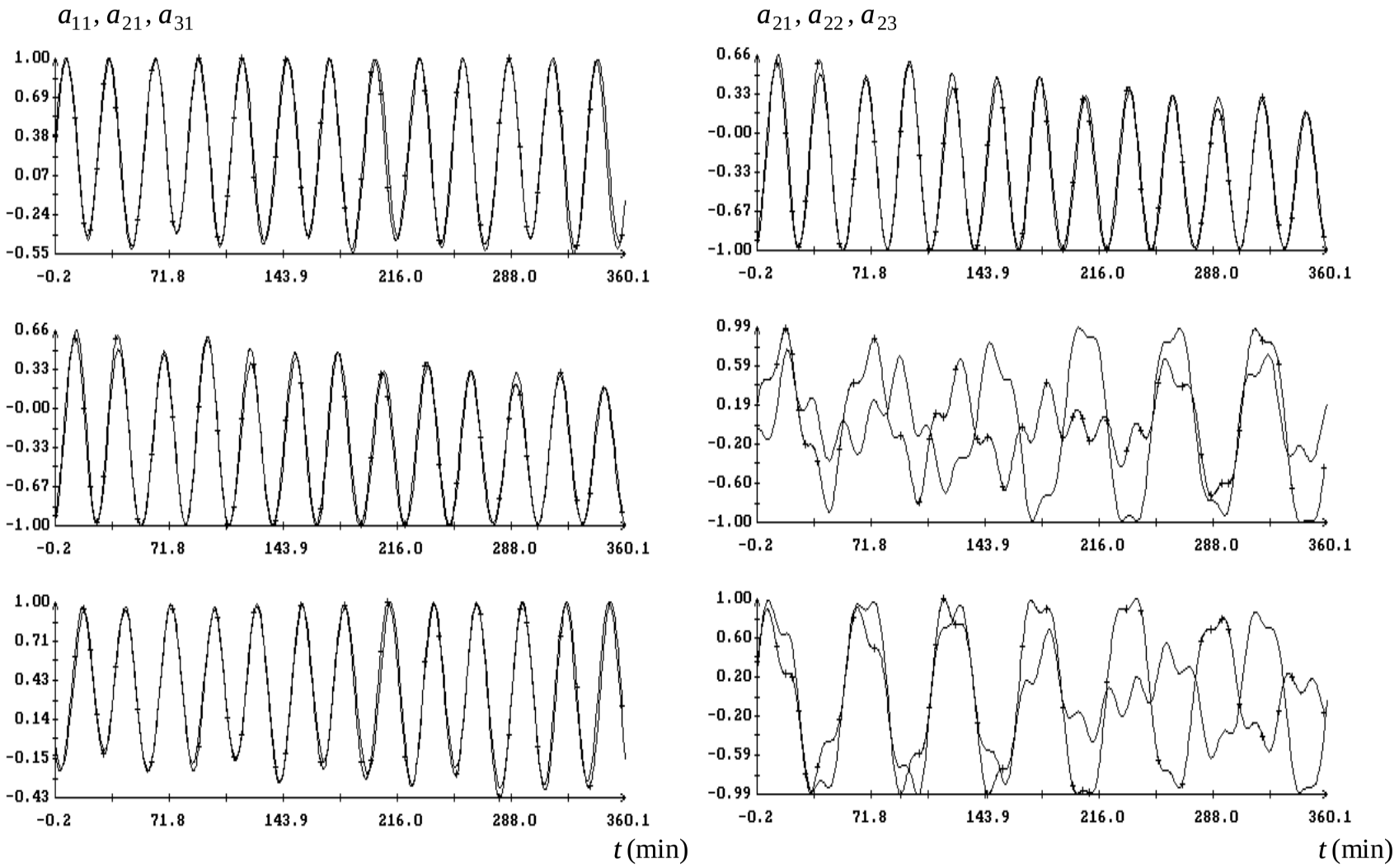

Fig. 8c. The instant $t = 0$ in the plots corresponds to $t_0 + t$, $t_0 =$19:12:15 UTC 24.09.2007, $t = -1$s.